Modelling and analysis of local field potentials for studying the function of cortical circuits

Gaute T. Einevoll[1], Christoph Kayser[2,3], Nikos K. Logothetis[4,5] and Stefano Panzeri[2,6]

Abstract | The past decade has witnessed a renewed interest in cortical local field potentials (LFPs) — that is, extracellularly recorded potentials with frequencies of up to ~500 Hz. This is due to both the advent of multielectrodes, which has enabled recording of LFPs at tens to hundreds of sites simultaneously, and the insight that LFPs offer a unique window into key integrative synaptic processes in cortical populations. However, owing to its numerous potential neural sources, the LFP is more difficult to interpret than are spikes. Careful mathematical modelling and analysis are needed to take full advantage of the opportunities that this signal offers in understanding signal processing in cortical circuits and, ultimately, the neural basis of perception and cognition.

[1]*Department of Mathematical Sciences and Technology, Norwegian University of Life Sciences, 1432 Ås, Norway.*
[2]*Institute of Neuroscience and Psychology, University of Glasgow, Glasgow, G12 8QB, UK.*
[3]*Bernstein Center for Computational Neuroscience, 72076 Tübingen, Germany.*
[4]*Max Planck Institute for Biological Cybernetics, Spemannstrasse 38, 72076 Tübingen, Germany.*
[5]*Division of Imaging Science and Biomedical Engineering, University of Manchester, Manchester, M13 9PT, UK.*
[6]*Center for Neuroscience and Cognitive Systems, Istituto Italiano di Tecnologia, Via Bettini 31, 38068 Rovereto, Italy.*
Correspondence to G.T.E. and S.P.
e-mails: Gaute.Einevoll@umb.no; Stefano.Panzeri@glasgow.ac.uk
doi:10.1038/nrn3599

Electrical signals from the cortical surface of animals were recorded as early as 1875 (REF. 1), 50 years before the advent of electroencephalography (EEG)[2]. Subsequent work revealed that the high-frequency part (above ~500 Hz) of the recorded potentials provides information about the spiking activity of neurons located around the electrode[3]. By contrast, the part of the signal that has frequencies below ~500 Hz, the so-called 'local field potential' (LFP), was found more difficult to interpret in terms of the underlying neural activity. Although the introduction of current source density (CSD) analysis in the 1950s[4] rejuvenated the use of the LFP in the following decades[5–7], interest decreased in the 1980s and 1990s, probably owing to the focus on new single-neuron techniques (for example, patch-clamp recordings) and on understanding the link between single-neuron activity and perception.

Recently, the interest in LFPs has undergone a resurgence. Key reasons are the growing capacity for streaming continuous data from multiple electrodes and the development of multicontact electrodes for high-density recordings across areas and laminae[8–12]. Further, the LFP captures key integrative synaptic processes that cannot be measured by observing the spiking activity of a few neurons alone. Several studies have used LFPs to investigate cortical network mechanisms involved in sensory processing[13–30], motor planning[31,32] and higher cognitive processes, including attention, memory and perception[33–37]. The LFP is also a promising signal for steering neuroprosthetic devices[38–41] and for monitoring neural activity in human recordings[42] because they are more easily and stably recorded in chronic settings than are spikes.

However, the use of the LFP signal comes with an important caveat. Because multiple neuronal processes contribute to the LFP, the signal is inherently ambiguous and more difficult to interpret than spikes. Here, we argue that this ambiguity can, at least in part, be resolved by developing computational methods of analysis and modelling that are able to disambiguate the different neural contributions to the LFP. Developing such mathematical tools is a thus a key priority of systems-level computational neuroscience.

To achieve this goal, it is crucial to have a good understanding of the 'measurement physics' of LFPs — that is, the link between neural activity and what is measured. The past decade has seen the refinement of a well-founded biophysical forward-modelling scheme that is based on volume conductor theory[43,44] to incorporate detailed reconstructed neuronal morphologies in precise calculations of extracellular potentials — both spikes[45–52] and LFPs[19,49,50,53–56]. (The word 'forward' denotes that the extracellular potentials are modelled from neural transmembrane currents; inverse modelling, by contrast, estimates neural currents from recorded potentials.) By using this tool, systematic investigations of the link between the recorded LFPs and various types of underlying neural activity can be pursued, and realistic data for the development and validation of methods for LFP analysis can be produced[12,49,57,58].

Current source density
The net volume density of transmembrane currents (including the capacitive membrane currents) entering the extracellular domain in a small volume of neural tissue.

Forward-modelling scheme
A scheme in which models are used to compute physical quantities (such as the extracellular potentials from synaptic neural activity) measured in experiments. Forward models are also known as 'generative models'.

In this Review, we discuss, on the basis of recent biophysical and neurobiological insights, how LFPs can be mathematically modelled and analysed in order to disentangle the contributing neural processes. We first outline the neural origin of cortical LFPs and the prospects for forward modelling of LFPs that stem from cortical network activity. We then discuss the various currently available methods for the interpretation of measured LFPs and spike–LFP relationships and, last, argue for a systematic effort to combine analysis and modelling of LFPs more deeply so as to take full advantage of the opportunities that this signal offers in understanding signal processing in cortical circuits.

LFPs from single neurons

Extracellular potentials arise from transmembrane currents passing through cellular membranes in the vicinity of the electrode[5,44,59,60]. For cortical LFPs, contributions from synaptic inputs appear to be the dominant component[7,19,49]. Their biophysical origin is well understood in the framework of volume conductor theory[59], and a forward-modelling scheme based on multicompartmental neuron models has been established[44,45,49,53–55] (BOX 1). Modelling studies based on this scheme have provided important insights into how LFPs from synaptic input currents (and their accompanying return currents) vary with a neuron's dendritic morphology and the positions of the synapse and recording electrode[44,53] (FIG. 1). These studies have shown that the sign, shape and amplitude of contributions to the LFP strongly depend on the recording position. For example, the LFP from an excitatory synaptic current onto an apical branch of a pyramidal neuron (FIG. 1Aa) is negative close to the synapse but positive

Box 1 | A biophysical forward-modelling scheme for LFPs

The local field potential (LFP) arises from transmembrane currents passing through cellular membranes in the vicinity of the electrode. Its biophysical origin is well understood in the framework of volume conductor theory[59], in which the extracellular medium is treated as a three-dimensional continuum, and extracellular electrical potentials are generated by cellular transmembrane currents. In this theory, single-compartment models do not generate extracellular potentials, and multicompartmental modelling must consequently be used to study LFPs[45,49,53–55]. The fundamental formula that describes the contribution of the activity in a multicompartmental neuron model to the extracellular potential ϕ[44,45,89] is:

$$\phi(\mathbf{r}_e, t) = \frac{1}{4\pi\sigma}\sum_{n=1}^{N}\frac{I_n(t)}{|\mathbf{r}_e - \mathbf{r}_n|} \quad (1)$$

Here, $I_n(t)$ denotes the transmembrane current (including the capacitive membrane current) in compartment n positioned at $\mathbf{r}_n$, $\mathbf{r}_e$ is the position of the electrode tip, the sum includes all N compartments, and σ is the extracellular conductivity. This formula, which is mathematically identical to Coulomb's law but has a different physical interpretation, implies that the LFP contribution from a transmembrane current will be inversely proportional to the distance between the compartment and the electrode. The extracellular conductivity σ reflects the ease with which ions can move in the convoluted extracellular medium. This parameter must in practice be determined in separate experiments, and for cortical grey matter it is around 0.3–0.4 S m^{-1} (REFS 70,100,157).

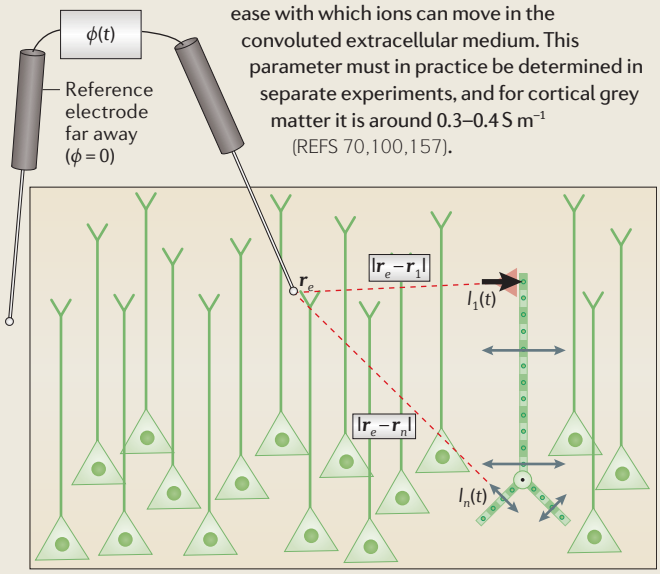

The figure illustrates how the LFP from a single excitatory apical input (red triangle) onto a schematically illustrated pyramidal neuron embedded in cortical neural tissue is calculated in this modelling scheme. The black arrow indicates the transmembrane current from the synapse itself, and the grey arrows indicate the transmembrane return currents. The point-source approximation[45,48] assumes that all transmembrane currents enter the extracellular space from a single point (indicated by the dots in each compartment of the neuron), whereas in the more commonly used line-source approximation[45,48], these currents are assumed to be evenly distributed along lines at the cylindrical axes of dendritic compartments (not shown). The above formula relies on a set of assumptions and approximations, including the use of quasistatic approximation of Maxwell's equations in which electrical and magnetic fields are effectively decoupled[100] and the assumption of an infinite volume conductor in which the electrical conductivity σ is ohmic (that is, no capacitive properties so that σ is real[59,70]), frequency-independent[70], homogeneous[157] and isotropic (that is, the same in all directions). For many applications, these assumptions seem warranted. However, the forward-modelling scheme can be generalized to incorporate situations in which one or more of these are assumptions are unfulfilled — for example, anisotropic conductivity in the cortex[157], conductivity jumps at cortical boundaries[19,57,157] or, if warranted, frequency-dependent impedance σ[68] (see REFS 75,89 for a discussion).

In the standard cable theory underlying multicompartmental modelling, the principle of charge conservation implies that the total sum of the transmembrane currents across all compartments (including capacitive currents) has to be zero at all times, implying that neural current monopoles should not exist[60,158]. However, a recent *in vivo* study challenged this view by reporting substantial contributions of monopole moments to mesoscopic LFP and electroencephalography signals recorded in the rat barrel cortex[67]. This interpretation was later challenged[159] by suggesting that the observed unbalanced current source density (CSD) stemmed either from the difficulty in incorporating entire membrane surfaces of all neurons in the experimental volume of interest (thus implying a genuine CSD unbalance) or from the difficulties in estimating CSDs from real data (for example, owing to incorrect assumptions about the spatial distribution of neural activity or detailed electrode positions). This objection and alternative interpretation have subsequently been questioned as well[160,161]. Some authors have suggested that the shunting of electrical currents through blood vessels or other non-neural tissue, or potential non-ohmic tissue properties could at least in principle play a part[67,162]. In our view, a useful aspect of this debate is that it raises the awareness of the technical pitfalls that may occur when estimating CSDs from experimental data.

Inverse modelling
Inversion of models refers to the selection of the best model (given some empirical data) and making probabilistic estimations of the parameters of that model. Models obtained with an inversion process are called 'inverse models'.

Multicompartmental neuron models
Neuron models in which dendrites and/or axons are divided into several compartments so that the membrane potential throughout each compartment can be assumed to be the same.

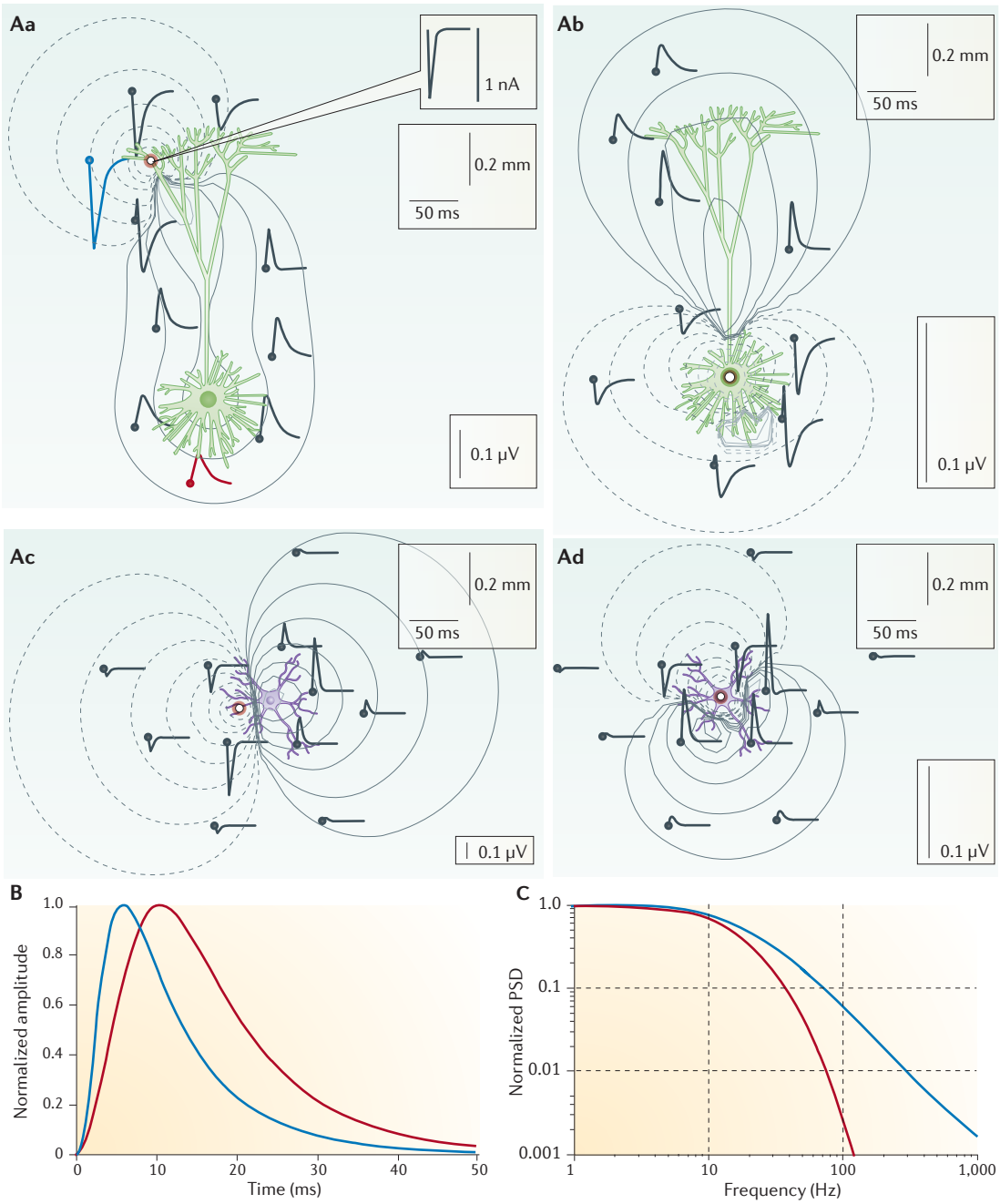

Figure 1 | **Calculated LFPs following synaptic activation of single neurons.** **A** | Local field potentials (LFPs) generated by single neurons critically depend on the neuronal morphology and positions of the synapses and recording electrodes. Here, this is illustrated by results from a modelling study involving activation by a single excitatory synapse (white circle) onto an apical branch (**Aa**) and onto the soma (**Ab**), respectively, of a reconstructed layer 5 pyramidal neuron, and onto a distal branch (**Ac**) and onto the soma (**Ad**) of a reconstructed layer 4 stellate cell. Both cells are from the cat visual cortex[173]. The inset in panel **Aa** shows the injected synaptic current. Extracellular potentials (thick solid traces) at selected spatial positions (marked with dots on trace starting points) are shown in 50 ms windows. Grey contour lines indicate the maximal extracellular potential (the LFP) amplitudes. Contour plots are logarithmic, and the LFP amplitude decays by a factor of two between each contour line. Solid contour lines indicate positive values for the LFP amplitude; dashed contour lines indicate negative values of the LFP amplitude. **B** | Normalized LFP magnitudes recorded close to the synapse (blue) and soma (red), respectively (as shown in panel **Aa**), illustrating the 'intrinsic dendritic filtering' effect[53], which is reflected here in the observation that the maximum amplitude of LFPs recorded close to the synapse occurs earlier than the maximum amplitude of LFPs recorded close to the soma. **C** | The power-spectral density (PSD) of LFP signals is shown at the same positions as in part **B** when white-noise (flat band) currents are injected into the apical synapse depicted in panel **Aa**. This illustrates the same effect directly in the frequency domain: that is, that the LFP measured close to the soma is more low-pass filtered than the LFP measured close to the synapse. Panels **Aa**–**Ad** are modified, with permission, from REF. 53 © (2010) Springer.

around the soma, where the accompanying return currents are strong (owing to the large surface area of dendrites in the soma region). A similar synapse onto the basal dendrites results in a dipole-like contribution of opposite polarity, with negative currents around the soma and positive currents at the apical dendrites (FIG. 1Ab). Positive currents leaving the extracellular medium — for example, positive charges entering neurons — are conventionally termed current sinks, whereas positive currents entering the extracellular medium are termed current sources.

The cortical pyramidal neurons in FIG. 1Aa,Ab have a characteristic open-field structure in which the synaptic input currents and resulting return currents may be substantially separated in space[61]. This implies a sizable current dipole, and it is thought that a superposition of many such open-field generators dominates cortical LFPs. LFPs that are generated by individual synaptic inputs onto cortical stellate cells (which have a spherically symmetrical dendritic arborization[43,61,62]) similarly generate dipole-like potentials orientated along the axis that is defined by the synapse and soma (FIG. 1Ac,Ad). The LFPs generated by many synaptic inputs onto such neurons are expected to largely cancel out when they are superimposed; such neurons are thought to have a so called closed-field configuration with a small net contribution to the LFP. Although this may suggest that stellate neurons contribute little to the recorded LFP, the cancellation of multiple contributions crucially depends on the simultaneous presence of evenly distributed currents. There may thus be situations in which stellate neurons substantially contribute to the LFP: for example, in subcortical structures such as the striatum or the thalamus, where pyramidal neurons are either absent or lack a preferred orientation.

Another key qualitative feature of the LFP is that signals close to the apical synapse (FIG. 1Aa) have 'narrower' temporal traces (that is, they have higher temporal frequencies) than do signals close to the soma, which are dominated by return currents in the soma region (FIG. 1B,C). This temporal filtering is also revealed by the delay of a few milliseconds of the peak times of the positive LFPs around the soma region compared with the negative LFPs around the active synapse[53] (FIG. 1B). Such 'intrinsic dendritic filtering' (REFS 48,53,55) arises from the cable properties of spatially extended neuronal structures. The shift in peak time reflects the temporal change in the spatial distribution of transmembrane return currents following onset of the synaptic current: it takes a few milliseconds for the steady-state current pattern to arise. Such a temporal filtering effect, which will attenuate certain frequencies in the input signal more than others, applies to all signals that are generated by transmembrane currents and thus has key implications for the interpretation of not only LFP power spectra[50,53,55] but also electrocorticography (ECoG)[63] and EEG power spectra[64,65]. Frequency filtering by the extracellular medium — for example, owing to diffusive processes[66] or ion buffering in biochemical processes[67]— might add to this phenomenon, but the impact of this on the recorded signals is a subject of debate[65–75].

To date, biophysical forward models for LFPs have mostly focused on passive neuron models, and only a few recent studies have considered models that include dendrites with active ion channels[50,56]. Such active conductances may crucially change the spatiotemporal distribution of LFPs generated by synaptic inputs. In addition, modelling studies have focused on pyramidal or stellate excitatory neurons and neglected contributions from inhibitory neurons, which constitute about one-fifth of cortical neurons[76]. However, the growing number of morphologically reconstructed and publicly available neurons (see, for example, NeuroMorpho.org) and new computational tools such as LFPy (see LFPy on the INCF Software Center website) implementing the forward-modelling scheme presented here (BOX 1) have now set the stage for a systematic investigation of the contributions to the LFP from different neuron types as well as LFPs generated by populations composed of multiple neuron types, as encountered in real cortical circuits.

Contributions to LFPs from other sources. Although synaptic input and the associated return currents may dominate cortical LFPs[7,19,49], spikes also contribute to the signal[49,50,77,78]. Even fast sodium spikes contribute to extracellular potentials with frequencies as low as 100 Hz[48], and slower phenomena such as calcium spikes[79] and spike afterhyperpolarization[80] further contribute to low-frequency LFP components[81]. As any transmembrane current will generate an extracellular potential, glial cells may also contribute to the LFP. However, their contribution is mainly expected at very low frequencies (less than 0.1 Hz[81]). Again, biophysical modelling will be essential in assessing these contributions to observed cortical LFPs across the various frequency bands.

Network activity underlying cortical LFPs

How local is the cortical LFP? Despite many years of research, the neural origin of recorded LFP signals — that is, the network activity that generates the signal — is still not fully understood. Although cortical LFPs seem to be dominated by synaptic currents and their accompanying return currents, the question of how local the signal is — that is, the spatial extent of the cortical region that generates a recorded LFP — is still vigorously discussed. Knowing this spatial reach is crucial for, for example, inferring the role of specific localized populations in computations and network function. Experimental studies have yielded apparently conflicting results, with estimates for the spatial reach ranging from a few hundred micrometres to several millimetres[25,34,35,82–84]. A recent modelling study[54] showed that these observations can be reconciled by assuming that the contributions from the single-neuron LFP generators were more synchronized in some of these studies than in others.

This study[54] investigated disc-like laminar populations of pyramidal neurons surrounding a recording electrode. When these neurons receive synaptic inputs, their LFP contributions add up linearly to produce the net population LFP. Everything else being equal, a neuron close to the electrode contributes more to the population LFP than a neuron further away. However, geometrical reasoning

Current sinks
Transmembrane currents that leave the extracellular domain and enter cells (including capacitive membrane currents).

Current sources
Transmembrane currents that enter the extracellular domain from the interior of cells (including capacitive membrane currents).

Open-field structure
A geometrical arrangement of synaptic inputs onto neurons in which, on average, there is a substantial spatial distance between synaptic currents and the bulk of the return currents, allowing for the generation of a large dipolar local field potential contribution (for example, apical inputs onto a population of large pyramidal neurons).

Closed-field configuration
A geometrical arrangement of synaptic inputs onto neurons in which, on average, there is no preferred orientation of spatial patterns of synaptic input currents and return current, giving a very small dipolar local field potential contribution.

implies that with a constant density of neurons in the disc-like population, the number of neurons at a particular distance from the electrode increases linearly with the distance. Hence, the relative contributions from the rings of neurons at different radial distances, and thus the spatial reach, depend on the 'competition' between these two opposing effects. Biophysical forward modelling[54] revealed that, for uncorrelated synaptic LFP sources, the spatial reach (defined as the radius around the electrode containing the neuronal sources that provide 95% of the LFP amplitude) was about 200 micrometres — roughly the lateral extent of the basal dendrites of the model neurons. This result held for all neuronal morphologies and synaptic distributions. By contrast, for correlated neural LFP sources, which were induced by driving the neurons in the populations with correlated synaptic inputs, the situation was very different: here, distant sources dominated owing to a 'constructive interference' effect between the single-neuron LFP sources (analogous to water-wave interference in physics), and the LFP signal increased without bounds with increasing population size. The spatial reach of a recorded LFP is thus mainly set by the spatial extent of the pool of surrounding, correlated neural sources[54,55,85].

Thus, the synaptic connectivity in cortical networks affects LFPs in two ways. First, it determines the spike-train statistics in the network and thus the correlation pattern of synaptic inputs. Second, the spatial distribution of synapses onto the neurons determines how the synaptic input correlations are 'translated' into the correlation structure of the individual LFP contributions that together set up the population LFP. In the modelling study[54], correlated synaptic inputs onto either basal or apical dendrites of pyramidal neurons resulted in strongly correlated single-neuron LFP sources and thus a strong amplification of the population LFP. By contrast, when the same synapses were homogeneously distributed over the dendrites, the single-neuron LFPs were weakly correlated and the population LFP was of much smaller amplitude.

The correlation level also determines the vertical LFP profile: correlated (and spatially asymmetrical) synaptic inputs generate a dipole-like LFP profile that spans the full vertical extent of the neural population, whereas homogeneous and/or uncorrelated inputs generate an LFP that is localized around the position of the synaptic inputs[55].

Interpretation of correlated LFPs. The interpretation of recorded LFPs and comparisons across studies are particularly challenging because LFPs strongly depend on the correlation pattern of synaptic inputs, and the synaptic correlation pattern depends on the set of activated anatomical connections — and hence on the kind of sensory stimuli used, the cognitive, or attentional load, or the experimental preparation (alert versus anaesthetized). Fortunately, the predictions from biophysical forward modelling can help such interpretations. For example, cortical multisite recordings show that LFPs recorded several hundreds of micrometres apart may be highly correlated[26,86]. Biophysical forward modelling[54] rules out that such correlated LFPs may be generated by uncorrelated synaptic inputs combined with volume conduction, as the spatial reach of LFPs generated by uncorrelated inputs would only be around 200 micrometres. Hence, correlated LFPs across much larger distances must arise either from two populations (each surrounding an electrode) that receive common or correlated synaptic inputs (for example, common thalamocortical drive), or from a single correlated population (possibly surrounding one of the electrodes) with an LFP that extends to electrodes that are positioned outside the active population through volume conduction. The modelling study[54] demonstrated the viability of the latter possibility, as it showed that the LFP measured 1 millimetre or more outside a correlated population may be larger than the LFP measured inside the same population when the neuronal LFP sources receive uncorrelated synaptic input (FIG. 2a). However, in this second scenario, the LFP recorded by the electrodes outside the correlated population should have a much smaller amplitude than the LFP within the correlated population; this is something that can be experimentally assessed.

Frequency-dependent features of LFPs. Experimental studies have shown that not only the amplitude but also the tuning to sensory features[35,82,87,88] and the amount of sensory information[20] vary across frequency bands in cortical LFPs. Therefore, another important question in interpreting LFPs is how the various frequency components of the spike firing rates generated by a cortical network are converted into corresponding frequency components of the LFP. The answer is that this conversion depends on at least two effects[55]. The first is the (predominantly) low-pass intrinsic dendritic filtering explained above[48,53,89]. The second is another low-pass filtering effect, as shown in a recent modelling study[55]: a higher proportion of the temporal correlations of presynaptic spike trains are 'translated' into correlations of single-neuron LFP contributions for low frequencies than for high frequencies. As a consequence, the boosting of the LFP signal by correlated synaptic inputs will be strongest for the lowest frequencies[55]. Note that this low-frequency amplification does not necessarily limit the stimulus information contained in high-frequency LFP signals, which can reflect important processes for sensory representations[90].

Modelling of LFPs from cortical networks

Computational models of LFPs will become increasingly important for the development and validation of methods for analysing and interpreting recorded LFPs. Here, we discuss how LFPs can be computed in comprehensive network simulations.

Because multicompartment neuron models are required for realistic forward modelling (BOX 1), an obvious approach is to build a virtual circuit that is based on populations of reconstructed cortical neurons and that emulates the known morphology, physiology and connectivity of the network of interest as much as possible[56,91,92] (also see The Human Brain Project website). However, such models are computationally demanding, and tuning the many model parameters in multicompartmental

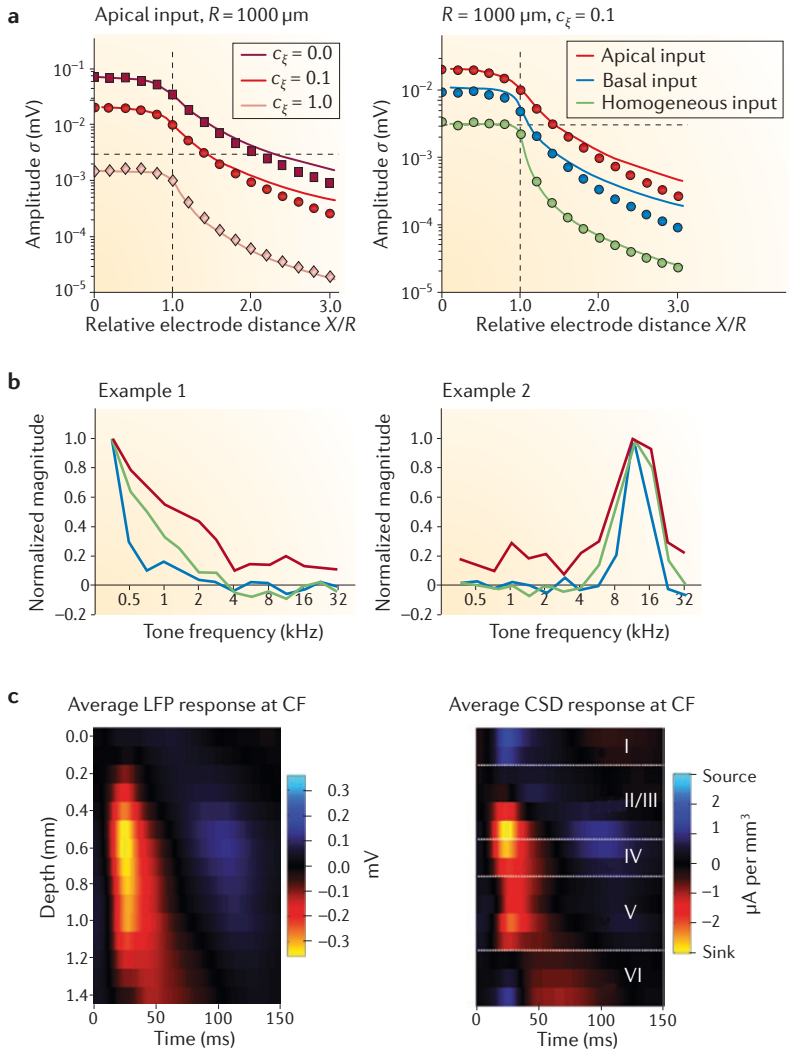

Figure 2 | **Spatial localization of CSD versus the LFP.** This figure illustrates the higher spatial resolution of current source density (CSD) compared with that of local field potentials (LFPs). **a** | Decay in the lateral direction of an LFP inside and outside a synaptically activated model population of layer 5 pyramidal cells with population radius $R = 1$ mm (x-axis units reported as a ratio between lateral distance X and population radius R). Curves and symbols correspond to results obtained from a simplified model and comprehensive numerical simulations, respectively; see REF. 54 for details. Although, as per definition, the CSD is essentially confined to a cylinder of the same size (demarcated by the vertical dashed line at $X/R = 1$ in the plot), the LFP extends far outside the population. Both the level of correlation (left panel; $c_\zeta = 0$ means uncorrelated and $c_\zeta = 1$ means fully correlated) and the spatial distribution of synaptic inputs (right panel; apical, basal or homogeneous) strongly affect how far the LFP will spread[54]. **b** | Two examples of tuning curves of multiunit activity (MUA, blue), CSD (green) and LFP (red) from the macaque auditory cortex. CSD is computed here as a double spatial derivative. The width of the tuning curve of the CSD is narrower than that of the LFP and more closely resembles that of the neural firing (MUA). **c** | Trial-averaged LFP (left panel) and CSD depth profile (right panel), which are estimated with the inverse CSD (iCSD) method, for one example recording session in the primary auditory cortex (A1) of anaesthetized rats. Activity was recorded during presentation of tones at the preferred sound frequency of this particular cortical location. The superimposed white dotted lines indicate the estimated depth of cortical layer boundaries. The responses to tones quantified with iCSD show a much better spatial localization of early sinks and sources than those quantified using the LFP. CF, characteristic frequency. Part **a** is reproduced, with permission, from REF. 54 © (2011) Elsevier. Part **b** is reproduced, with permission, from REF. 84 © (2011) Elsevier. Part **c** is modified, with permission, from REF. 29 © (2011) Society for Neuroscience.

neurons is notoriously difficult. Most forward-modelling studies so far have therefore used simplified single-compartment integrate-and-fire neuron models[93]. Furthermore, most studies have focused on generic properties of homogenous networks; structured network models that mimic the laminar organization of cortical columns have only recently been developed[94,95].

Thus, a crucial methodological question is how to compute, from simplified networks of single-compartment neurons, an LFP proxy that preserves the dependence on position and time or frequency of the LFP obtained from multicompartment models as much as possible[22,27,96–99]. Several proxies for the LFP have been suggested, including pooled spike trains[98], average membrane potentials in neuronal populations[96,97] and sums of synaptic input currents onto pyramidal neurons[22,27]. None of these proxies can be expected to be generally valid for predicting cortical LFPs. One reason is that the vertical extent of the contributions from each population to the LFP is similar to the vertical extent of the dendrites (FIG. 1), and hence the net LFP at each location is a sum of positive and negative contributions from several overlapping neuronal populations that partially cancel each other out. This cancellation effect and the effect of intrinsic dendritic filtering[53,55,89] can only be captured with spatially extended multicompartmental models.

In forward modelling of EEG or magnetoencephalography signals, the distances between the neural sources and the recording sensors are so large that individual contributions to the signal can be well approximated by their current dipole moments and the well-established far-field dipolar expressions, in which the individual contributions decay with the square of the distance from the source[59,100]. Unfortunately, the single-neuron contribution to the LFP only reaches its far-field dipolar limit a millimetre or more away from the neuron[53], whereas dominant contributions to the recorded LFPs may come from neurons within a distance of a few hundred micrometres[54]. This implies that the far-field dipole approximation cannot a priori be assumed to be generally applicable when calculating the LFP. Similarly, the related two-monopole approximation for calculating LFPs, where the transmembrane currents are assumed to enter and exit only through two point-like somatic and dendritic compartments (with equal magnitude and opposite directions)[53,101,102], is inaccurate for distances of up to a few hundred micrometres from the neuronal somata[53].

At present, there are thus no validated methods for calculating LFPs in network simulations that are based on single-compartment model neurons. An important question for future research is to systematically address this issue by comparing various proxies for the LFP with ground-truth data from network models based on multicompartment models that are constructed from detailed dendritic morphologies.

CSD analysis of LFPs

We now turn our attention to the 'inverse' problem — namely, identifying the neural sources that contribute to the LFP from LFP data. The oldest and most widely

used method is CSD analysis. The CSD measures the net current density that enters or leaves the extracellular medium through cell membranes. It is, by definition, a more local measure than the LFP and therefore easier to interpret in terms of neural activity[4–7,57]. As the various neural elements that contribute transmembrane currents (dendrites, somata and axons) are entangled in a densely packed, intertwined structure, it is not possible — even with today's recording techniques — to estimate the detailed microscopic arrangement of individual transmembrane currents within the extracellular space. As a result, in practice, the CSD reflects the average transmembrane current on the scale of a few tens of micrometres.

Traditional CSD analysis. Over spatial scales of some hundred micrometres, neocortical tissue is, owing to its laminar organization, much more diversified along the vertical axis (that is, across layers) than in lateral directions. On the assumption that there is little lateral variation in neural activity, vertical CSD profiles have typically been estimated from simultaneous recordings of LFPs across the cortical laminae[13,14,17,23,29,57,84,103–105]. In this traditional CSD analysis, the key assumption is that the lateral variation of the LFP can be neglected so that the CSD can be estimated from a simple 'double spatial derivative' of the recordings along the vertical axis[6] (BOX 2). The physical intuition behind this mathematical relationship is as follows: the first LFP derivative gives the potential drop between the contacts and thus the extracellular current (assuming an ohmic medium), whereas the second derivative approximates the local current change that is due to transmembrane current sources or sinks. Although taking this double spatial derivative of the LFP yields a signal that is much more local (FIG. 2b), it does not always correctly estimate the spatial pattern of neural current sources. This may be the case in, for example, primary sensory cortices, where the stimulus-evoked activation pattern is often confined to a region of a few hundred micrometres[19,49,57,106,107]. In cases in which the sources violate the assumption of lateral homogeneity, the double-derivative estimate for the CSD may exhibit spurious current sinks and sources (BOX 2).

Inverse CSD analysis. The inverse CSD (iCSD) method[57] (BOX 2) goes beyond the assumption of constant LFPs in the lateral directions, as it allows more general assumptions for the geometrical distribution of CSD sources. This method first establishes a forward model to describe the field potential that is produced by localized currents under the assumed geometrical configuration of sources (BOX 2), and then inverts this model by means of a numerical matrix inversion to allow a direct calculation of localized current sources from the experimentally measured potentials. Unlike traditional CSD, the iCSD method can, in a straightforward manner, include any assumptions or a priori knowledge about the neural sources, such as the lateral size of columnar activity and discontinuities or direction-dependence of the extracellular conductivity; it can be applied to any geometrical arrangement of electrode contacts; and it can estimate the CSD at the positions of the electrode contacts at the boundary of the electrode[12,57,108]. This last point is particularly advantageous for CSD estimates that are based on three-dimensional electrode configurations, in which more than half of the contacts may be at the boundary[108]. The flexibility of iCSD in terms of the assumptions of size and positions of the CSD sources can be further enhanced by pairing iCSD with kernel techniques from machine learning[109].

Because of their higher spatial resolution and more direct biophysical interpretation, CSDs may reveal aspects of spatiotemporal cortical dynamics that simple spectral analysis of LFPs cannot[110,111]. An example is provided by a study of the encoding of complex sounds in the auditory cortex. Single-channel LFP analysis revealed the presence of informative phase resets of low-frequency LFPs (<12 Hz)[24,29] but could not identify the precise spatiotemporal pattern of the neural currents that induce these phase resets. By contrast, iCSD analysis revealed that most, if not all, of the stimulus-related information in LFP phases originated from discrete stimulus-locked 'CSD events', consisting of granular–superficial layer dipoles of short duration and large amplitude (FIG. 2c), that reliably reset the LFP phases[29]. These findings suggest that in the auditory cortex, the information provided by LFP phases results from transient, large-amplitude depolarization in thalamo-recipient layers of the cortex and illustrate the power of CSD analysis to disentangle the cross-laminar temporal activity patterns underlying sensory information processing.

Functional decomposition of LFPs

The LFP is traditionally decomposed and interpreted in the frequency domain. For example, Fourier analysis[112] allows the separation of frequency bands such as the widely used delta, theta, alpha, beta and gamma bands. The validity of this approach is supported by the observed associations of these band-limited power signals with distinct behavioural states or sensory inputs[20,113,114]. However, the definition of individual frequency bands is often largely arbitrary, based on heuristic criteria and varies substantially between studies.

One quantitative approach that can be used to define functionally meaningful bands is to quantify co-variations in amplitude across bands. If amplitude variations in one band are independent of amplitude variations in another, then these two bands probably capture different neural contributions to the LFP. Correlations among LFP bands can be computed across repeated presentations of a set of different experimental conditions, such as cognitive tasks or sensory stimuli. This procedure identifies boundaries between statistically independent frequency regions in the LFP and can hence be used to separate functionally distinct contributors to the LFP. The disentanglement of independent neural contributions to the LFP can be facilitated by introducing sufficiently high variation in the experimental conditions, as larger variations are more likely to engage distinct neural processes. For example, in sensory areas, such approaches greatly benefit from the use of naturalistic stimuli.

Single-compartment integrate-and-fire neuron models
Neuron models in which the membrane potential is assumed to be the same across the soma and dendrites.

Current dipole moments
Mathematical measures of spatial distribution of transmembrane currents across the neuronal membrane.

Far-field dipole expressions
Mathematical expressions for the extracellular potential generated by a current dipole source for distances far away from the dipole. In this limit, the potential will be proportional to the current dipole moment and inversely proportional to the square of the distance.

Ground-truth data
In its original context in remote sensing, this term refers to data recorded on location (on the ground) to validate methods for analysing remote-sensing imaging data. In the context of local field potential (LFP) data, it refers to data obtained using the detailed biophysical forward-modelling scheme in which the neural activity is fully known, allowing for validation of methods for analysis of the LFP and prediction of LFPs in cortical network simulations.

Traditional CSD analysis
(Traditional current source density analysis). A method for estimating the depth profile of CSD across cortical laminae based on taking the 'double spatial derivative' of multielectrode local field potential (LFP) data, inherently assuming the LFP (and CSD) to be constant in the lateral directions.

Inverse CSD
(Inverse current source density). A method for estimating CSD from multielectrode local field potential (LFP) data based on numerical inversion of the forward model, linking CSD distributions to measured LFPs.

Box 2 | **Traditional CSD analysis versus iCSD analysis**

The standard way of analysing local field potential (LFP) data used to be by means of current source density (CSD) analysis[4–7,57]. The principle of CSD analysis is as follows (see the figure, part **a**): when a columnar population of pyramidal neurons receives a volley of excitatory input onto, say, their apical dendrites (left panel), a characteristic sink–source CSD pattern is generated inside the column (middle panel). This CSD distribution will in turn set up a spatially more-diffuse LFP pattern that can be recorded by, in this case, a laminar multielectrode (right panel). The challenge of CSD analysis is then to estimate the underlying CSD distribution from these laminar LFP recordings.

The mathematical link between the CSD and the electrical potential ϕ — that is, the CSD forward model — is, in analogy to the forward model formula in BOX 1, given by the integral[5]:

$$\phi(\mathbf{r}_e) = \frac{1}{4\pi\sigma}\iiint_V \frac{C(\mathbf{r})}{|\mathbf{r}_e - \mathbf{r}|}\, d^3r \qquad (2)$$

Here, $\mathbf{r}_e$ denotes the position of the electrode contact, C denotes the CSD, and the subscript V on the triple integral denotes volume integration over all transmembrane currents. The corresponding inverse formula is given by the Poisson equation:

$$\sigma\left(\frac{\partial^2\phi}{\partial^2 x} + \frac{\partial^2\phi}{\partial^2 y} + \frac{\partial^2\phi}{\partial^2 z}\right) = C(x, y, z) \qquad (3)$$

Although this differential equation applies when the conductivity σ is constant and the same in all directions (x, y and z), the formula can easily be generalized to the case with position-dependent $\sigma = \sigma(\mathbf{r})$ or anisotropic extracellular conductivity[89].

As neocortical tissue has a laminar organization, the common assumption has been that most variation of neural activity is in the vertical direction, and depth-resolved CSD profiles have been estimated from recordings of LFPs across the cortical laminae[4,5]. In traditional CSD analysis, the CSD at the various electrode contact positions z_j is thus estimated by the discrete double spatial derivative[5,6]:

$$C(z_j) = -\sigma\left(\frac{\phi(z_j + \delta) - 2\phi(z_j) + \phi(z_j - \delta)}{\delta^2}\right) \qquad (4)$$

assuming no variation of the CSD in the lateral (x and y) directions (compare to equation 3). Here, δ is the inter-electrode contact distance. When this is not fulfilled (as for the columnar CSD in part **a** of the figure), the traditional CSD analysis cannot be trusted.

As shown already in the 1970s in a pioneering study[5], traditional CSD analysis will predict spurious sinks and sources around the true sink–source pair (see the figure, part **b**, top panels) when the columnar activity is confined within a cylinder. The sizes and shapes of these spurious sinks and sources will depend on the cylindrical diameters d and heights h (see the figure, part **b**, top right and bottom panels). Further, the magnitude of the true sinks and sources will be underestimated[57]. In the inverse CSD (iCSD) method[12,57,108], this problem is avoided by using the forward solution in equation 2 to incorporate the assumed size of the columnar activity directly into the CSD estimator. An example application is shown in part **c** of the figure. This shows analysis of the CSD from a model population of pyramidal neurons, mimicking a layer 5 population in the rat barrel cortex that receives transient apical synaptic excitation. Here, the traditional CSD analysis predicts spurious sinks and source (middle panel), whereas the iCSD method — in this case the spline version[57] — assuming an activity diameter of 0.4 mm corresponding to the size of the true cortical column, gives CSD estimates (right panel) very similar to the ground truth (left panel). Est, estimated. Part **a** is modified, with permission, from REF. 154 © (2012) Springer. Part **b** is modified, with permission, from REF. 5 © (1975) The American Physiological Society. Part **c** is modified, with permission, from REF. 49 © (2008) Springer.

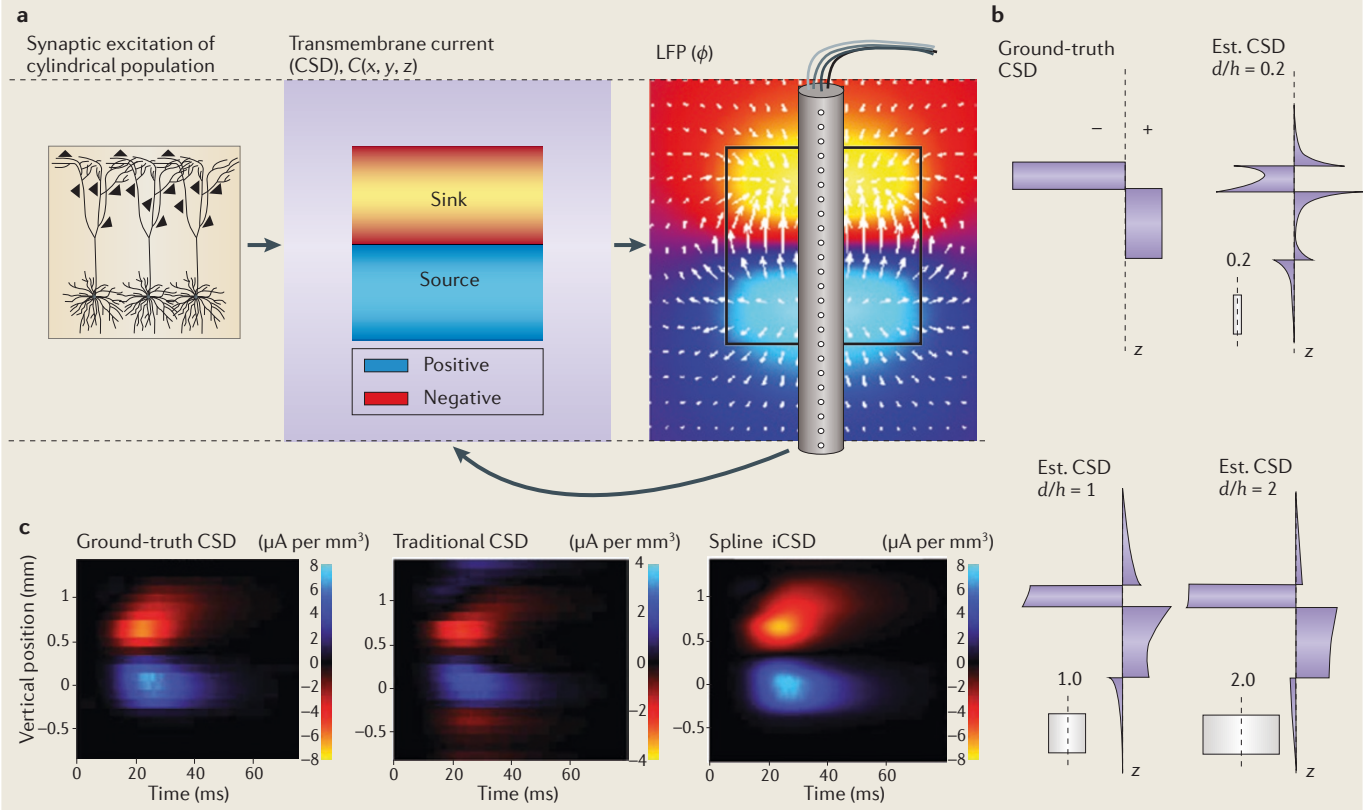

Band-limited power
The total power (square of the absolute value or amplitude) of a signal that can be approximated by a sum of sine waves with frequencies that are restricted to a relatively narrow range ('frequency band').

Laminar multielectrode
(Also known as a linear multielectrode). An electrode used for making extracellular electrical recordings. It has many contacts orientated along a single shaft and is typically inserted perpendicularly into the cortex to span several cortical layers.

Signal correlations
A measure of correlations between neural signals attributable to the external correlate. The correlations are quantified as the correlation of tuning of two neural signals to the external conditions (for example, the correlation of the trial-averaged response profile across different external conditions).

Noise correlations
A measure of correlations between neural signals that cannot possibly be attributed to the external correlate. The correlations are quantified as the correlation between two neural signals at a fixed external stimulus or behavioural condition.

Mutual information
A measure of the amount of knowledge about a stochastic variable (for example, an external stimulus) that can be extracted from the single-trial observation of another stochastic variable (for example, a neural signal). It is measured in bits — one bit corresponds to a reduction of uncertainty by a factor of two.

Information maximizing band-separation method
A method that determines frequency band boundaries so that they maximize the information about external conditions (such as sensory stimuli or cognitive tasks) extracted from the resulting band-separated neural response.

Two types of correlations among frequency bands have been considered: signal correlations and noise correlations[20,115–117]. Signal correlations (see Supplementary information S1 (box)) reflect the similarity of different frequency bands in their tuning to external conditions. An example of a signal correlation is the correlation of trial-averaged response profiles across different external conditions. Noise correlations (see Supplementary information S1 (box)) reflect the trial-by-trial co-variations between different frequency bands after discounting for their similarities in tuning to the external conditions. Despite the name, noise correlations not only capture correlations in what may be neural noise but may also include the effect of neurophysiologically important processes, such as diffuse neuromodulatory inputs. The analysis of signal and noise correlations becomes especially powerful when it is combined with additional analytical tools, such as mutual information[118,119], that quantify both the amount and the nature of the information about external conditions carried by each frequency band. This enables not only the identification of the boundaries between statistically independent bands but also the identification of the specific aspects of the external conditions that are reflected by the activity in each LFP component.

For example, studies on the encoding of naturalistic visual information in the primate visual cortex revealed a distinct pattern of signal and noise correlations (FIG. 3b) between LFP bands: frequencies between 10 Hz and 24 Hz exhibit high noise correlations but low signal correlations and carry little stimulus information (FIG. 3a). This indicates that signals in this frequency range are generated by common processes that are unrelated to the visual stimuli — for example, diffuse neuromodulatory inputs. By contrast, frequencies in the gamma range exhibited high visual information and also had large signal correlations among them, indicating that activities at these frequencies have a common component that is stimulus-driven[20]: for example, through a set of thalamic inputs. Most strikingly, these data revealed that frequency bands above ~50 Hz and frequency bands below ~50 Hz shared neither signal correlations nor noise correlations, indicating that they act as independent visual information channels and probably originate from separate neural processes.

Determining functional boundaries between frequency bands is more challenging when there is an incomplete dissociation of signal correlations and noise correlations. For example, although it is widely accepted that gamma oscillations (typically defined as the 30–80 Hz and 40–100 Hz bands in awake and anaesthetized animals, respectively) reflect network oscillations mediated by rhythmic inhibition[120], it remains unclear whether the 'high-gamma' band (80–120 Hz and 100–150 Hz in awake and anaesthetized animals, respectively) reflects sustained rhythmic activity that is similar to the classical gamma cycle but operating at higher frequencies, or reflects brief bursts of power associated with spikes that are generated near the electrode[77]. Differentiating between these two possibilities is difficult because gamma oscillations and spike rates are often correlated across sensory or cognitive manipulations. One proposed approach to separate partly correlated bands is the information maximizing band-separation method (see Supplementary information S1 (box)). This approach determines the boundary that maximizes the amount of information about the external conditions of interest (for example, the sensory stimuli) that is gained after splitting the spectrum into separate bands[121]. The information-maximizing band-separation method can identify the previously discussed boundaries between frequency bands with zero signal and noise correlations. In addition, it can reveal useful boundaries between bands that carry information that is maximally complementary to each band in cases when a perfect separation between fully uncorrelated bands is not possible (see Supplementary information S1 (box)). For example, when the information maximizing band-separation method was applied to data from the primate visual cortex, it revealed that segregating the LFP into three frequency bands of 1–50 Hz (low-frequency band), 50–100 Hz (gamma band) and >100 Hz (high-gamma band) maximizes the information about the visual stimuli that it carries (FIG. 3c). This agrees with the independence of frequencies above and below 50 Hz discussed above, and suggests that these gamma and high-gamma bands reflect partly distinct neural processes[122].

A limitation of the traditional LFP band-separation techniques (such as Fourier analysis) is that they decompose LFPs into a set of oscillatory functions that cannot possibly capture transient fluctuations of extracellular potentials, such as fluctuations that reflect phasic responses that occur after stimulus onset or that occur around sharp neural events such as spikes or ripples. The matching pursuit algorithm[123,124] provides a powerful approach to decompose the LFP into both transient and oscillatory functions. Application of this algorithm to visual stimuli in the primary visual cortex (V1) of awake monkeys showed that high-gamma LFPs (70–120 Hz) could be decomposed mostly into transient components that were tightly coupled to spike times. This suggests that high-gamma LFPs reflect spiking activity rather than genuine network oscillations and thus capture neural processes that are different from those captured by gamma-band (30–80 Hz) oscillations.

To understand the functions and inter-relationships of distinct oscillatory networks, it is important to identify not only the most important frequency bands but also the timing of events within different bands. For example, the timing of an increase in power in a given band is commonly detected by band-pass filtering the LFP followed by application of a threshold to obtain an estimate of the signal power. However, this approach may not be sufficiently sensitive to discern quantitatively distinct, simultaneously occurring oscillatory events that may reflect the activity of distinct subnetworks (for example, gamma oscillations or ripple oscillations in the hippocampus). Such potentially distinct neural events can be classified using robust unsupervised feature-extraction algorithms, such as non-negative matrix factorization[125], to cluster the spectra measured around event times. Application of this

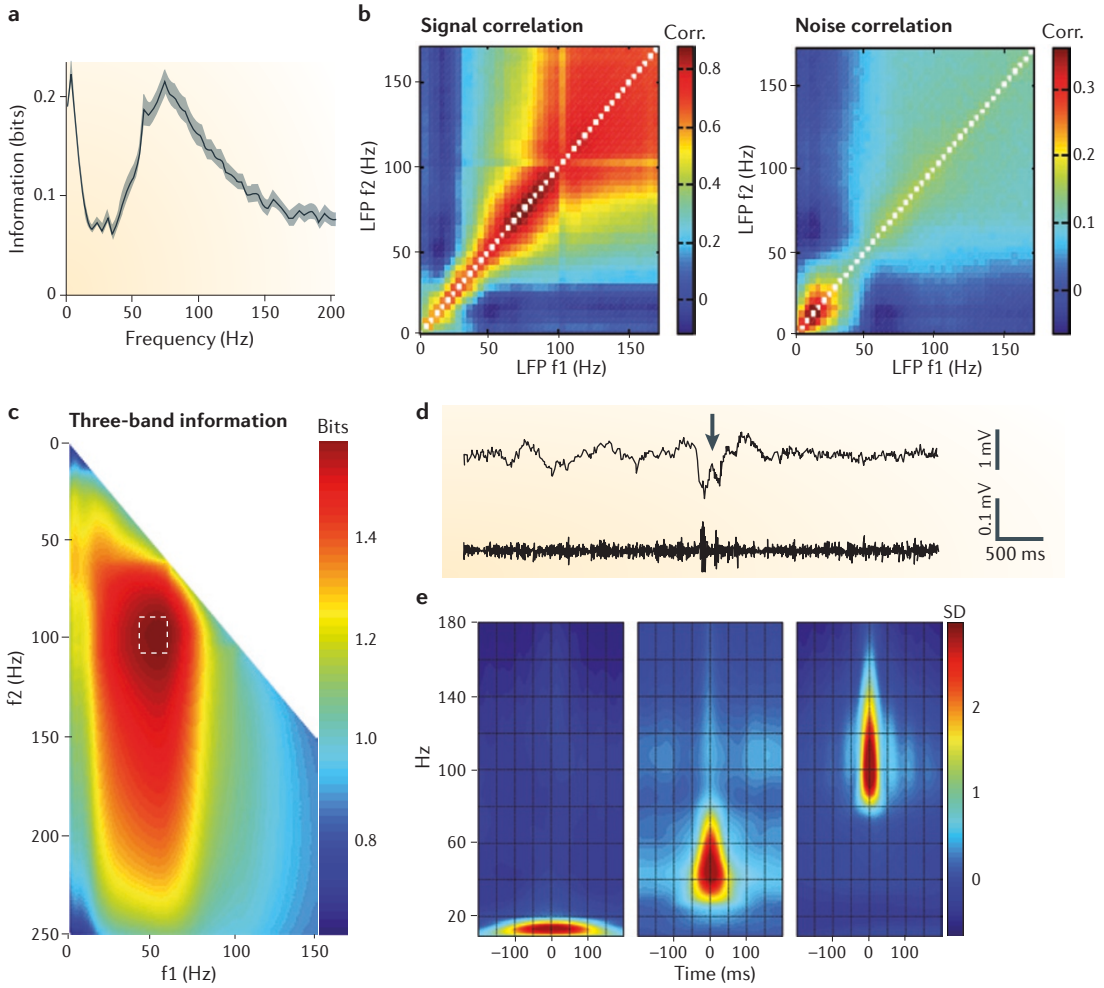

Figure 3 | **Separating functionally distinct frequency bands in LFP recordings.** This figure illustrates how mathematical techniques based on information theoretical principles or on non-negative matrix factorization may help to separate the local field potential (LFP) into distinct frequency bands and spectral events. Panels **a**–**c** show results from data from the macaque primary visual cortex (V1) obtained during presentation of commercial movie clips. **a** | Information about the movie carried by the LFP power at different frequencies. **b** | Pearson signal correlation (left) and Pearson noise correlation (right) of the LFP power for each pair of frequencies (f1 and f2). **c** | Partitioning these LFP responses into three bands using the information maximizing band-separation method. This panel plots the information about the visual stimuli carried by the joint observation of LFP power in the three bands B1 = 0 Hz–f1, B2 = f1–f2 and B3 = f2–250 Hz as a function of the boundary frequencies f1 and f2 varied between 0 and 250 Hz. The dashed rectangle indicates the position of the boundaries that maximize information (interquartile range across the population). Panels **d** and **e** show data from the primate hippocampus and illustrate how to separate neural events into well-defined spectral clusters. **d** | An example of a recording trace containing one sharp wave–ripple complex (SPW-R). The top line shows the broadband (0.05–500 Hz) LFP signal, and the bottom line shows its band-passed (80–180 Hz) derivative. The SPW-R is indicated by the arrow. **e** | After all SPW-Rs were identified, the LFP spectrograms around each event were clustered into three classes (hippocampal sigma, gamma and ripple bands), and the average of spectrograms of each clustered class was plotted, showing the time–frequency distribution of each type of event around the time of SPW-R event detection. Corr, correlation. Parts **a** and **b** are modified, with permission, from REF. 20 © (2008) Society for Neuroscience. Part **c** is modified, with permission, from REF. 121 © (2012) Elsevier. Parts **d** and **e** are modified, with permission, from REF. 126 © (2012) Macmillan Publishers Ltd. All rights reserved.

Matching pursuit
An algorithm that iteratively decomposes a signal into waveforms selected from a set of functions, including functions extended in time but narrow in frequency, and functions brief in time but broad in frequency.

Non-negative matrix factorization
(NMF). An algorithm that learns, with an unsupervised technique, how to decompose non-negative datasets into parts or modules, the linear sum of which approximates the data. It can then be used to group data samples into clusters based on their decompositions in terms of these parts.

method to hippocampal recordings robustly separated sharp-wave ripple complexes into three distinct event categories in the frequency domains of 8–22 Hz (hippocampal sigma waves), 25–75 Hz (hippocampal gamma) and 80–180 Hz (ripple) bands[126] (FIG. 3d,e).

It may be particularly fruitful to apply such separation methods in conjunction with experimental stimulation methods that can activate distinct neural elements or pathways associated with specific signals of interest. For example, optogenetic tools now enable the induction of patterns of oscillatory activity at distinct rhythms in selected neural populations and the de-activation of selected neurons over distinct timescales[127,128]. In addition, electrical stimulation can induce rhythmic activity in local neural populations[129] and in the human brain on a larger scale[130].

Box 3 | **Spike-triggered average of the LFP**

The spike-triggered average of the local field potential (stLFP)[26,107,131] is often used to quantify the postsynaptic responses at one location of spiking activity at another location. This interpretation of the stLFP rests on the causal assumption that the stLFP mostly reflects the effect of the spikes recorded at earlier times on the LFPs. This assumption is valid when studying feedforward monosynaptic connections[106,107] — for example, when examining primary visual cortical LFPs that are triggered by spikes recorded from simultaneously recorded geniculate neurons and that are generated by a single geniculate axon through the depth of the cortex (see the figure, part **a**). However, the interpretation is more complicated when spikes and LFPs are recorded at multiple sites within a recurrent cortical network. Here, although stLFPs are largest after the spike, they also capture non-causal components that occurred before the spike[26,163], as shown in part **b** of the figure, which shows plots of stLFPs computed from spikes and LFPs recorded in the primary visual cortex within a range of inter-electrode contact distances ((δ) indicated in units of millimetres).

One complicating factor is that LFPs can also causally contribute to spikes. For example, LFPs capture network rhythms such as low-frequency or gamma oscillations, which can bias the likelihood of spiking[164]. The resulting locking of spikes to oscillations is captured in spike–LFP associations, and this makes it more difficult to interpret stLFPs[164]. One way to tease apart the interplay between spikes and network rhythms is to compute directional measures of causal interactions[165,166]. These measures reveal a marked frequency dependence of the causal relationships from spikes to the LFP, from the LFP to spikes and between different rhythms within the LFP. Typically, the dominant direction of causation is in the direction from low-amplitude, high-frequency components (spikes or LFP gamma band) to high-amplitude, low-frequency LFP components; the gamma phase is more effective than spikes themselves at predicting spiking responses at other electrodes[167]. Low-amplitude rhythms in the gamma band have a particularly high impact on feedforward communication[168,169]. This indicates that simply considering the amplitude of spike–LFP (or LFP–LFP) interaction measures may not always accurately measure the strength of the underlying biophysical interactions between sites. When using spike–LFP measures to draw conclusions about network interactions, it may be necessary to tease apart the causal contribution of spikes to LFPs and of LFPs to spikes that occur at different LFP oscillation frequencies.

Other confounding factors in spike–LFP relationships include the contribution from low-frequency components of spike waveforms to the LFP[50] (which can be reduced by techniques such as matching pursuit[77] or Bayesian spike removal algorithms[170]), and the contribution from spatiotemporal correlations of spikes within the network to the stLFP[163]. This confounding factor can be addressed by computing measures (such as the impulse response of LFPs to spikes) that can discount the effect of spatiotemporal correlations[163,171]. These linear descriptions of the dependence of LFPs on spiking activity at other sites are not only useful as measures of postsynaptic responses but also as a means to empirically characterize how LFPs are generated within the cortical circuit. It is particularly useful to characterize how LFP generation may depend on, for example, the network excitability, which in turn can be modulated by factors such as arousal and attention[172]. Part **a** of the figure is reproduced, with persmission, from REF. 107 © (2011) Macmillan Publishers Ltd. All rights reserved. Part **b** of the figure is modified, with permission, from REF. 164 © (2011) Society for Neuroscience.

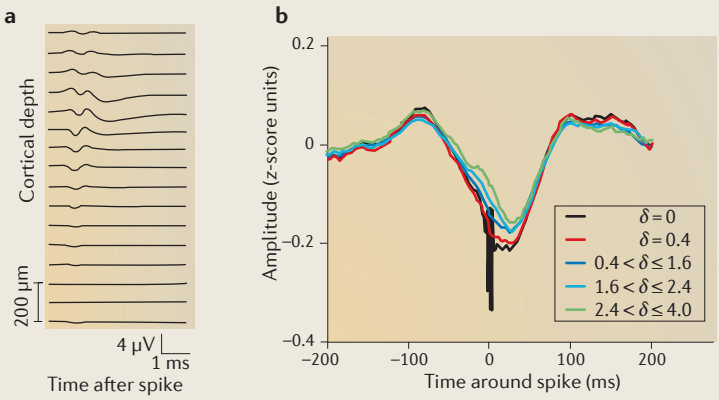

Analysis of spike–LFP relationships

The joint analysis of simultaneously recorded LFPs and spikes provides an additional window into cortical activity. For example, relationships between spikes and LFPs measured at different sites can be used to assess the strength of synaptic activity at one cortical site (reflected in the LFP at that site) caused by spiking at the same or at another location. One measure used to characterize interactions between spikes and LFPs at different sites is the spike-triggered average of the LFP (stLFP)[26,107,131]. Interpreting the stLFP in terms of neural interactions rests on the assumption that the stLFP mostly reflects the effect of the recorded spikes on LFPs: that is, that the LFP is generated by a spike recorded at earlier times (a 'causal interpretation'). Although stLFPs are unambiguous when studying feedforward monosynaptic connections[106,107], their interpretation is more complicated when both spikes and the LFP are recorded at multiple sites within a recurrent cortical network (BOX 3). Here, non-causal stLFP contributions may arise, because the stLFP captures not only signals arising from synaptic activity directly associated with the spike but captures all kinds of activity locked to the spike. This makes the estimation of effective connectivity from the stLFP — and from spike–LFP relationships in general — a major challenge that remains unresolved. Some of the difficulties involved are discussed in BOX 3.

Considering spike–LFP relationships also improves the interpretation of laminar recordings. The CSD is a more local measure than the LFP (as explained above), but its interpretation is nevertheless non-trivial. For example, an observed negative CSD (sink) in cortical layer 2 may be due to excitatory synaptic currents going into dendrites of the basal region of layer 2 pyramidal neurons and/or due to excitatory synaptic currents going into the apical dendrites of layer 5 pyramidal cells. The sink could also stem from return currents that accompany basal inhibition of the layer 5 neuron. Thus, a research goal is to go beyond CSD analysis and instead attempt decomposition of cortical LFPs in terms of contributions from different neural populations[13,14,58,132,133]. Laminar population analysis (LPA)[19] is one method that involves joint analysis of LFPs and spikes to constrain the decomposition. In LPA, the basic assumption is that the LFP can be decomposed into its causal contributions from the firing of spikes in laminar populations. This population firing activity is in turn measured using multiunit activity (MUA)[49,103]. LPA applied on laminar-electrode data from the rat barrel cortex[19] provided identification of the vertical positions of physiologically relevant laminar cortical populations, estimates of the firing rates of these populations and estimates of the spatiotemporal LFP profiles following action-potential firing in the individual populations. This approach, combined with an LFP template-fitting technique that was based on LFP population templates that were calculated using biophysical forward modelling (BOX 1), allowed a map of the active synaptic connections between the identified populations to be estimated[19].

Fitting network models to LFP data

Once forward models of neural networks are able to produce realistic LFPs, they can be fitted to experimental data (a procedure often denoted as 'model inversion') using statistical techniques such as Bayesian model inversion[134–136]. The best-fit models can then be used to interpret experimental LFPs (for example, to individuate the contributions to network dynamics from the different neural pathways that generate the LFP, or to estimate values of key network parameters — such as physiological synaptic parameters or the input to the considered network — that may not be directly measurable from the spiking activity of a small number of neurons). Thereby, computer models could be used not only to validate specific methods for LFP or CSD analysis but also to constrain the interpretation of experimentally recorded LFPs.

A promising way to test methods of LFP analysis and prediction is to use models with recurrent excitatory and inhibitory populations. These allow the assessment of how LFP quantities derived from the model — such as the spectrum of LFP oscillations, cross-spectra or spike–LFP relationships — depend on network parameters.

One class of such models is neural mass models[137] (see Supplementary information S2 (box)) (also called firing-rate models), in which the dynamical variables represent average population activities. In such models, LFPs can be approximated by neural mass variables, and Bayesian statistics can be used to infer both synaptic parameters and effective connection strengths in neural circuits[136,138]. A limitation of current neural mass models is that they cannot generate the full range of network states that are observed in the cortex (for example, weakly and strongly synchronized states, and regular and irregular firing states); by contrast, these states can be generated using network models that include the dynamics of individual neurons[139,140]. An important line for future research is to develop approximations for LFPs and other experimentally measurable quantities for models that can generate a range of realistic dynamical states. Systematic derivations of neural mass-like models from spiking-neuron dynamics[141–145] are promising developments in this direction. Further, just as for the spiking-neuron network models described above, a systematic comparison between various proxies for the LFP that is based on neural mass variables and ground-truth data found from detailed multicompartment models should be pursued.

Although model fitting and advanced analyses have not often been used together so far, a more systematic combination of complementary advanced analysis and model-based approaches will be crucial to advance the interpretation of LFPs[146]. For example, analytical separation methods (such as the information-based methods described above) cannot by themselves identify the precise cellular or anatomical mechanisms that generate the individual frequency components of the LFP. However, they can extract candidate signals of interest for subsequent modelling of the underlying neural information-processing mechanisms. In turn, these methods can quantitatively test model predictions — for example, predictions on how information about sensory variables is distributed across temporal frequencies or across cortical laminae.

For example, in studies of encoding of naturalistic visual stimuli in the primary visual cortex, information analysis[20] identified two frequency bands (low frequency (1–20 Hz) and gamma band (50–100 Hz)) that each carried independent sensory information. Subsequent modelling studies of networks with excitatory and inhibitory neurons[22,27] provided a quantitative explanation of how each of these frequency bands could be generated by different aspects of the dynamics of the same network. The results suggested that gamma-range LFPs are generated by inhibitory–excitatory neural interactions and encode the amplitude of the instantaneous thalamic input, whereas the low-frequency LFP encodes slow variations in the sensory input by entrainment of the network dynamics at the corresponding frequency.

Another example of how coupling biophysical forward modelling with analytical tools can yield new insights about information processing in cortical circuits comes from REF. 147. Here, the LPA analysis of laminar LFPs was first used to identify how the laminar populations excite each other synaptically, and the data were then fitted to neural mass models in order to interpret time-resolved population firing rates in terms of the underlying thalamocortical and intracortical signal propagation[147].

Conclusions and future directions

The recent development of LFP analysis approaches provides us with a better description and understanding of the LFP, and in particular of how the LFP may provide information about sensory or cognitive processes of interest that complements the information obtained by analysis of spikes only. Modelling approaches that take into account the biophysical processes and the structural details and microconnectivity of various brain regions can further increase the information that can be extracted from LFPs. We see the mathematical quantitative understanding of how the LFP is generated and of how it should be analysed as important factors for successfully using the LFP to study the function of neural circuits.

One key challenge for computational neuroscientists is to fully tease apart the aggregate response that constitutes an LFP into potentially independent signal components. Despite unequivocal progress, this remains difficult for several reasons. The first is that recordings carried out in a stimulus- or task-relevant area tend to show co-variations between all aspects of measured electrical signals — from MUA to LFPs — and some of the characteristics of the stimulus or the task. This high interdependency of many components of the signal makes their separation challenging. The second reason is that many existing attempts to objectively separate different bands rely on classifying changes of signal power in a restricted frequency region. This approach does not easily accommodate the complexity of frequency-dependent properties that are either unrelated to power or related to cross-frequency or global spectral properties[148,149]. For example, phase–amplitude and phase–phase inter-frequency coupling are powerful indicators of inter-areal communication or neuromodulatory effects, but their generality, the conditions of their appearance and their relation to local events are largely

Directional measures of causal interactions
Statistical techniques to evaluate the causal effect of a group of simultaneously recorded signals onto another group of simultaneously recorded signals.

Spike-triggered average of the LFP
(Spike-triggered average of the local field potential). The value of the LFP as a function of time around the spike emission times, averaged over all observations of spikes. It is used to quantify the stereotypical values of mean fields that are measured near the observation of a spike.

Laminar population analysis
(LPA). A method for estimating cortical laminar population profiles, time-resolved laminar population firing rates and synaptic connection patterns between laminar populations based on joint modelling of multiunit activity and local field potentials from multielectrode recordings.

Multiunit activity
(MUA). The high-frequency part of recorded extracellular potentials (above approximately 500 Hz) used as a measure of action-potential spiking from neurons in the vicinity of electrode. MUA can be estimated by identifying individual spikes by thresholding the high-pass signal (sometimes with the additional step of convolving the resulting spike time series with a temporal kernel), or alternatively it can be estimated by first high-pass filtering the signal in the range of more than ~700–800 Hz and then rectifying it.

Bayesian model inversion
A statistical technique that estimates the model parameters that best fit some given empirical data.

Neural mass models
Models of neural network dynamics in which activity of a neural ensemble is summarized with a single variable: the mean of the density of ensemble activity. They are also known as firing-rate models.

unknown. The interpretation of coupling between different LFP components is even more problematic when episodes of coupling appear at irregular epochs or are only transiently related to sensory or cognitive functions. It seems that a much-needed first step is to develop procedures by which the LFP signal can be split into components that characterize the state of local microcircuits. Of importance may be the application of system-identification and statistical learning methods[150,151] that permit unbiased, minimally overlapping clustering of signal-spectra, that enable the extraction of distinct functional components carrying information specific to the experimental question (for example, sensory representations, cognitive tasks) or that directly relate to specific laminar neuronal populations.

Future progress also requires methods for identifying and clustering neurophysiological events (for example, sequences of population activation) that occur during specific tasks or conditions of interest. Robust classification and repeatable cross-frequency interactions may enable the separation of feedforward signals from feedback signals and the identification of neuromodulatory processes. Our optimism for rapid progress along these lines rests on the established biophysical link between the activity of individual neurons and extracellular potentials, including LFPs. It is now possible to build comprehensive network models for individual cortical columns or even larger chunks of tissue and to predict spikes, LFPs and spike–LFP relationships at different positions[49] with accuracy, and this will be crucial for thorough testing of candidate cortical network models against experimental data[56,91,92,94,95,152]. Validated models could be used to provide a more precise interpretation of network states in terms of LFPs recordings. For example, these models could be used to interpret phase values (that is, phases of excitability cycles) of cortical oscillations at different depths in terms of phases of excitability cycles. Another important application of such models is to provide biophysically realistic ground-truth data that can be used both to judge the accuracy of methods for analysis of LFP and spike–LFP relationships[49] and to understand how analytical separation methods and inverse modelling can be best coupled together. Crucial for this progress is a coordinated, collaborative effort to develop open-source software tools for the generation and application of benchmarking test data (in the spirit of, for example, recent initiatives of the International Neuroinformatics Coordinating Facility (see the Spike Sorting Evaluation Project website) to facilitate validation of automatic spike-sorting algorithms[153]).

A second key challenge arises from the brain's complex structure; brain functions probably emerge from the concerted, context-dependent operations of its microscopic and macroscopic networks. The organization and operational principles of such complex systems may be best investigated by using multimodal approaches, including concurrent measurements on multiple spatiotemporal scales coupled with manipulation of neural activations. Such multimodal recording methodologies — potentially combined with electrical or optogenetic stimulation — promise to characterize the state of widespread networks by measuring the correlational and causal relationships of activity in individual structures. A great challenge for computational neuroscientists is therefore to develop a methodology that takes full advantage of these recordings. This includes supplementing integrative models of cortical microcircuits with biophysics-based model predictions of optical signals (for example, voltage-sensitive dye imaging and two-photon calcium imaging) and magnetic resonance measurement signals (functional MRI)[74,154], and developing the analytical methodology to study information flow and emergent properties in large systems. This will probably require the introduction of mathematical methods from the causal theory of intervention[155,156] to study the propagation of information following stimulation; of methods from analysis of complex systems to study state changes in high-dimensional variable spaces; and of methods that can be used in systems with strong feedback, in which there is no clear direction of information flow. Progress in computational tools for studying such emergent properties may yield unprecedented insight into the workings of the brain at the systems level.

The ease with which LFPs can be recorded and the richness of the signal makes it ideal for use in prosthetic devices and investigating the neural activity underlying cognition. But only by advancing and using appropriate computational tools will we be able to uncover the stories told by this signal.

1. Caton, R. The electric currents of the brain. *BMJ* **2**, 278 (1875).
2. Berger, H. Über das elektreenkephalogramm des menschen. *Arch. Psychiatr. Nervenkr.* **87**, 527–570 (1929) (in German).
3. Adrian, E. D. & Moruzzi, G. Impulses in the pyramidal tract. *J. Physiol.* **97**, 153–199 (1939).
4. Pitts, W. in *Cybernetics Trans. 9th Conf. Josiah Macy Found.* 159–166 (Diaphanes, 1952).
5. Nicholson, C. & Freeman, J. A. Theory of current source-density analysis and determination of conductivity tensor for anuran cerebellum. *J. Neurophysiol.* **38**, 356–368 (1975).
6. Freeman, J. A. & Nicholson, C. Experimental optimization of current source-density technique for anuran cerebellum. *J. Neurophysiol.* **38**, 369–382 (1975).
7. Mitzdorf, U. Current source-density method and application in cat cerebral cortex: investigation of evoked potentials and EEG phenomena. *Physiol. Rev.* **65**, 37–100 (1985).
8. Normann, R. A., Maynard, E. M., Rousche, P. J. & Warren, D. J. A neural interface for a cortical vision prosthesis. *Vision Res.* **39**, 2577–2587 (1999).
9. Buzsaki, G. Large-scale recording of neuronal ensembles. *Nature Neurosci.* **7**, 446–451 (2004).
10. Kipke, D. R. *et al.* Advanced neurotechnologies for chronic neural interfaces: new horizons and clinical opportunities. *J. Neurosci.* **28**, 11830–11838 (2008).
11. Du, J., Blanche, T. J., Harrison, R. R., Lester, H. A. & Masmanidis, S. C. Multiplexed, high density electrophysiology with nanofabricated neural probes. *PLoS ONE* **6**, e26204 (2011).
12. Leski, S. *et al.* Inverse current source density method in two dimensions: inferring neural activation from multielectrode recordings. *Neuroinformatics* **9**, 401–425 (2011).
13. Di, S., Baumgartner, C. & Barth, D. S. Laminar analysis of extracellular field potentials in rat vibrissa/barrel cortex. *J. Neurophysiol.* **63**, 832–840 (1990).
14. Barth, D. S. & Di, S. Laminar excitability cycles in neocortex. *J. Neurophysiol.* **65**, 891–898 (1991).
15. Kandel, A. & Buzsaki, G. Cellular-synaptic generation of sleep spindles, spike-and-wave discharges, and evoked thalamocortical responses in the neocortex of the rat. *J. Neurosci.* **17**, 6783–6797 (1997).
16. Schroeder, C. E., Mehta, A. D. & Givre, S. J. A spatiotemporal profile of visual system activation revealed by current source density analysis in the awake macaque. *Cereb. Cortex* **8**, 575–592 (1998).
17. Schroeder, C. E. *et al.* Somatosensory input to auditory association cortex in the macaque monkey. *J. Neurophysiol.* **85**, 1322–1327 (2001).
18. Henrie, J. A. & Shapley, R. LFP power spectra in V1 cortex: the graded effect of stimulus contrast. *J. Neurophysiol.* **94**, 479–490 (2005).
19. Einevoll, G. T. *et al.* Laminar population analysis: estimating firing rates and evoked synaptic activity from multielectrode recordings in rat barrel cortex. *J. Neurophysiol.* **97**, 2174–2190 (2007).

20. Belitski, A. *et al.* Low-frequency local field potentials and spikes in primary visual cortex convey independent visual information. *J. Neurosci.* **28**, 5696–5709 (2008).
The first study to document the sensory information content and the patterns of signal and noise correlations among the power of different LFP bands and to use these patterns to separate functionally different bands of LFPs.
21. Montemurro, M. A., Rasch, M. J., Murayama, Y., Logothetis, N. K. & Panzeri, S. Phase-of-firing coding of natural visual stimuli in primary visual cortex. *Curr. Biol.* **18**, 375–380 (2008).
22. Mazzoni, A., Panzeri, S., Logothetis, N. K. & Brunel, N. Encoding of naturalistic stimuli by local field potential spectra in networks of excitatory and inhibitory neurons. *PLoS Comput. Biol.* **4**, e1000239 (2008).
This study shows how to compute simple but effective LFP approximations from simulated recurrent networks of point-like integrate-and-fire neurons, and how to use these quantities to infer which neural pathways generate the information carried in each part of the LFP frequency spectrum.
23. Szymanski, F. D., Garcia-Lazaro, J. A. & Schnupp, J. W. Current source density profiles of stimulus-specific adaptation in rat auditory cortex. *J. Neurophysiol.* **102**, 1483–1490 (2009).
24. Kayser, C., Montemurro, M. A., Logothetis, N. K. & Panzeri, S. Spike-phase coding boosts and stabilizes information carried by spatial and temporal spike patterns. *Neuron* **61**, 597–608 (2009).
25. Katzner, S. *et al.* Local origin of field potentials in visual cortex. *Neuron* **61**, 35–41 (2009).
26. Nauhaus, I., Busse, L., Carandini, M. & Ringach, D. L. Stimulus contrast modulates functional connectivity in visual cortex. *Nature Neurosci.* **12**, 70–76 (2009).
27. Mazzoni, A., Whittingstall, K., Brunel, N., Logothetis, N. K. & Panzeri, S. Understanding the relationships between spike rate and delta/gamma frequency bands of LFPs and EEGs using a local cortical network model. *Neuroimage* **52**, 956–972 (2010).
28. Mazzoni, A., Brunel, N., Cavallari, S., Logothetis, N. K. & Panzeri, S. Cortical dynamics during naturalistic sensory stimulations: experiments and models. *J. Physiol.* **105**, 2–15 (2011).
29. Szymanski, F. D., Rabinowitz, N. C., Magri, C., Panzeri, S. & Schnupp, J. W. The laminar and temporal structure of stimulus information in the phase of field potentials of auditory cortex. *J. Neurosci.* **31**, 15787–15801 (2011).
30. Victor, J. D., Purpura, K., Katz, E. & Mao, B. Q. Population encoding of spatial-frequency, orientation, and color in macaque V1. *J. Neurophysiol.* **72**, 2151–2166 (1994).
31. Scherberger, H., Jarvis, M. R. & Andersen, R. A. Cortical local field potential encodes movement intentions in the posterior parietal cortex. *Neuron* **46**, 347–354 (2005).
32. Roux, S., Mackay, W. A. & Riehle, A. The pre-movement component of motor cortical local field potentials reflects the level of expectancy. *Behav. Brain Res.* **169**, 335–351 (2006).
33. Pesaran, B., Pezaris, J. S., Sahani, M., Mitra, P. P. & Andersen, R. A. Temporal structure in neuronal activity during working memory in macaque parietal cortex. *Nature Neurosci.* **5**, 805–811 (2002).
34. Kreiman, G. *et al.* Object selectivity of local field potentials and spikes in the macaque inferior temporal cortex. *Neuron* **49**, 433–445 (2006).
35. Liu, J. & Newsome, W. T. Local field potential in cortical area MT: stimulus tuning and behavioral correlations. *J. Neurosci.* **26**, 7779–7790 (2006).
36. Womelsdorf, T., Fries, P., Mitra, P. P. & Desimone, R. Gamma-band synchronization in visual cortex predicts speed of change detection. *Nature* **439**, 733–736 (2006).
37. Liebe, S., Hoerzer, G. M., Logothetis, N. K. & Rainer, G. Theta coupling between V4 and prefrontal cortex predicts visual short-term memory performance. *Nature Neurosci.* **15**, 456–462 (2012).
38. Mehring, C. *et al.* Inference of hand movements from local field potentials in monkey motor cortex. *Nature Neurosci.* **6**, 1253–1254 (2003).
39. Andersen, R. A., Musallam, S. & Pesaran, B. Selecting the signals for a brain–machine interface. *Curr. Opin. Neurobiol.* **14**, 720–726 (2004).
40. Rickert, J. *et al.* Encoding of movement direction in different frequency ranges of motor cortical local field potentials. *J. Neurosci.* **25**, 8815–8824 (2005).
41. Markowitz, D. A., Wong, Y. T., Gray, C. M. & Pesaran, B. Optimizing the decoding of movement goals from local field potentials in macaque cortex. *J. Neurosci.* **31**, 18412–18422 (2011).
42. Mukamel, R. & Fried, I. Human intracranial recordings and cognitive neuroscience. *Annu. Rev. Psychol.* **63**, 511–537 (2012).
43. Rall, W. Electrophysiology of a dendritic neuron model. *Biophys. J.* **2**, 145–167 (1962).
44. Rall, W. & Shepherd, G. M. Theoretical reconstruction of field potentials and dendrodendritic synaptic interactions in olfactory bulb. *J. Neurophysiol.* **31**, 884–915 (1968).
A pioneering study in which modelling of evoked extracellular potentials in the olfactory bulb was used to predict dendrodendritic interactions between mitral and granule cells.
45. Holt, G. R. & Koch, C. Electrical interactions via the extracellular potential near cell bodies. *J. Comput. Neurosci.* **6**, 169–184 (1999).
The first application of detailed reconstructed neuronal morphologies in biophysical forward modelling of extracellular potentials.
46. Gold, C., Henze, D. A. & Koch, C. Using extracellular action potential recordings to constrain compartmental models. *J. Comput. Neurosci.* **23**, 39–58 (2007).
47. Gold, C., Henze, D. A., Koch, C. & Buzsaki, G. On the origin of the extracellular action potential waveform: a modeling study. *J. Neurophysiol.* **95**, 3113–3128 (2006).
48. Pettersen, K. H. & Einevoll, G. T. Amplitude variability and extracellular low-pass filtering of neuronal spikes. *Biophys. J.* **94**, 784–802 (2008).
49. Pettersen, K. H., Hagen, E. & Einevoll, G. T. Estimation of population firing rates and current source densities from laminar electrode recordings. *J. Comput. Neurosci.* **24**, 291–313 (2008).
50. Schomburg, E. W., Anastassiou, C. A., Buzsaki, G. & Koch, C. The spiking component of oscillatory extracellular potentials in the rat hippocampus. *J. Neurosci.* **32**, 11798–11811 (2012).
51. Thorbergsson, P. T., Garwicz, M., Schouenborg, J. & Johansson, A. J. Computationally efficient simulation of extracellular recordings with multielectrode arrays. *J. Neurosci. Methods* **211**, 133–144 (2012).
52. Camunas-Mesa, L. A. & Quiroga, R. Q. A detailed and fast model of extracellular recordings. *Neural Comput.* **25**, 1191–1212 (2013).
53. Linden, H., Pettersen, K. H. & Einevoll, G. T. Intrinsic dendritic filtering gives low-pass power spectra of local field potentials. *J. Comput. Neurosci.* **29**, 423–444 (2010).
A detailed biophysical-modelling study of the contribution to the LFP from single neurons and how it depends on neuronal morphology and positions of the synapses and recording electrodes.
54. Linden, H. *et al.* Modeling the spatial reach of the LFP. *Neuron* **72**, 859–872 (2011).
A detailed biophysical-modelling study of the spatial locality of the LFP and how it depends on neuronal morphology, spatial distribution of synaptic inputs and, importantly, the level of correlation between the synaptic inputs driving the neurons in the vicinity of the recording electrode.
55. Leski, S., Linden, H., Tetzlaff, T., Pettersen, K. H. & Einevoll, G. T. Frequency dependence of signal power and spatial reach of the local field potential. *PLoS Comput. Biol.* **9**, e1003137 (2013).
56. Reimann, M. W. *et al.* A biophysically detailed model of neocortical local field potentials predicts the critical role of active membrane currents. *Neuron* **79**, 375–390 (2013).
This large-scale biophysical forward-modelling study provides a detailed simulation of the neural origin of the LFP in a model of a rodent neocortical column comprising very detailed morphological, anatomical and physiological information.
57. Pettersen, K. H., Devor, A., Ulbert, I., Dale, A. M. & Einevoll, G. T. Current-source density estimation based on inversion of electrostatic forward solution: effects of finite extent of neuronal activity and conductivity discontinuities. *J. Neurosci. Methods* **154**, 116–133 (2006).
An introduction of the iCSD method for estimation of CSD from multielectrode LFP recordings.
58. Gratiy, S. L., Devor, A., Einevoll, G. T. & Dale, A. M. On the estimation of population-specific synaptic currents from laminar multielectrode recordings. *Front. Neuroinform.* **5**, 32 (2011).
59. Nunez, P. L. & Srinivasan, R. *Electric Fields in the Brain. The Neurophysics of EEG* (Oxford Univ. Press, 2005).
60. Plonsey, R. & Barr, R. C. *Bioelectricity: a Quantitative Approach* 3rd edn (Springer, 2007).
61. Johnston, D. & Wu, S.-S. *Foundations of Cellular Neurophysiology* (MIT Press, 1995).
62. Lorente de Nó, R. Action potential of the motoneurons of the hypoglossus nucleus. *J. Cell Comp. Physiol.* **29**, 207–287 (1947).
63. Miller, K. J., Sorensen, L. B., Ojemann, J. G. & den Nijs, M. Power-law scaling in the brain surface electric potential. *PLoS Comput. Biol.* **5**, e1000609 (2009).
64. Freeman, W. J., Holmes, M. D., Burke, B. C. & Vanhatalo, S. Spatial spectra of scalp EEG and EMG from awake humans. *Clin. Neurophysiol.* **114**, 1053–1068 (2003).
65. Dehghani, N., Bedard, C., Cash, S. S., Halgren, E. & Destexhe, A. Comparative power spectral analysis of simultaneous elecroencephalographic and magnetoencephalographic recordings in humans suggests non-resistive extracellular media. *J. Comput. Neurosci.* **29**, 405–421 (2010).
66. Bedard, C. & Destexhe, A. Macroscopic models of local field potentials and the apparent 1/f noise in brain activity. *Biophys. J.* **96**, 2589–2603 (2009).
67. Riera, J. J. *et al.* Pitfalls in the dipolar model for the neocortical EEG sources. *J. Neurophysiol.* **108**, 956–975 (2012).
68. Bedard, C., Kroger, H. & Destexhe, A. Modeling extracellular field potentials and the frequency-filtering properties of extracellular space. *Biophys. J.* **86**, 1829–1842 (2004).
69. Bedard, C., Kroger, H. & Destexhe, A. Does the 1/f frequency scaling of brain signals reflect self-organized critical states? *Phys. Rev. Lett.* **97**, 118102 (2006).
70. Logothetis, N. K., Kayser, C. & Oeltermann, A. *In vivo* measurement of cortical impedance spectrum in monkeys: implications for signal propagation. *Neuron* **55**, 809–823 (2007).
71. Gabriel, S., Lau, R. W. & Gabriel, C. The dielectric properties of biological tissues: II. measurements in the frequency range 10 Hz to 20 GHz. *Phys. Med. Biol.* **41**, 2251–2269 (1996).
72. Gabriel, C., Peyman, A. & Grant, E. H. Electrical conductivity of tissue at frequencies below 1 MHz. *Phys. Med. Biol.* **54**, 4863–4878 (2009).
73. Bedard, C., Rodrigues, S., Roy, N., Contreras, D. & Destexhe, A. Evidence for frequency-dependent extracellular impedance from the transfer function between extracellular and intracellular potentials: intracellular-LFP transfer function. *J. Comput. Neurosci.* **29**, 389–403 (2010).
74. Brette, R. & Destexhe, A. (eds) *Handbook of Neural Activity Measurement* (Cambridge Univ. Press, 2012).
75. Bedard, C. & Destexhe, A. in *Handbook of Neural Activity Measurement* (eds Brette, R. & Destexhe, A.) 136–191 (Cambridge Univ. Press, 2012).
76. Braitenberg, V. & Schüz, A. *Cortex: Statistics and Geometry of Neuronal Connectivity* 2nd edn (Springer, 1998).
77. Ray, S. & Maunsell, J. H. Different origins of gamma rhythm and high-gamma activity in macaque visual cortex. *PLoS Biol.* **9**, e1000610 (2011).
A study using careful manipulations of visual stimuli and matching pursuit spectral analysis techniques to show how to separate contributions to the LFP of genuine gamma-band rhythms from the contribution of spike-related transients that could be incorrectly decomposed as rhythms using traditional signal-processing methods.
78. Scheffer-Teixeira, R., Belchior, H., Leao, R. N., Ribeiro, S. & Tort, A. B. On high-frequency field oscillations (> 100 Hz) and the spectral leakage of spiking activity. *J. Neurosci.* **33**, 1535–1539 (2013).
79. Stuart, G., Spruston, N. & Häusser, M. *Dendrites* 2nd edn (Oxford Univ. Press, 2007).
80. Buzsaki, G. *et al.* Nucleus basalis and thalamic control of neocortical activity in the freely moving rat. *J. Neurosci.* **8**, 4007–4026 (1988).
81. Buzsaki, G., Anastassiou, C. A. & Koch, C. The origin of extracellular fields and currents — EEG, ECoG, LFP and spikes. *Nature Rev. Neurosci.* **13**, 407–420 (2012).
82. Berens, P., Keliris, G. A., Ecker, A. S., Logothetis, N. K. & Tolias, A. S. Comparing the feature selectivity of the gamma-band of the local field potential and the underlying spiking activity in primate visual cortex. *Front. Syst. Neurosci.* **2**, 2 (2008).
83. Xing, D., Yeh, C. I. & Shapley, R. M. Spatial spread of the local field potential and its laminar variation in visual cortex. *J. Neurosci.* **29**, 11540–11549 (2009).

84. Kajikawa, Y. & Schroeder, C. E. How local is the local field potential? *Neuron* **72**, 847–858 (2011).
85. Einevoll, G. T., Linden, H., Tetzlaff, T., Leski, S. & Pettersen, K. H. in *Principles of Neural Coding* (eds Quian Quiroga, R. & Panzeri, S.) 37–59 (CRC Press, 2013).
86. Destexhe, A., Contreras, D. & Steriade, M. Spatiotemporal analysis of local field potentials and unit discharges in cat cerebral cortex during natural wake and sleep states. *J. Neurosci.* **19**, 4595–4608 (1999).
87. Salazar, R. F., Konig, P. & Kayser, C. Directed interactions between visual areas and their role in processing image structure and expectancy. *Eur. J. Neurosci.* **20**, 1391–1401 (2004).
88. Kayser, C., Petkov, C. I. & Logothetis, N. K. Tuning to sound frequency in auditory field potentials. *J. Neurophysiol.* **98**, 1806–1809 (2007).
89. Pettersen, K. H., Linden, H., Dale, A. M. & Einevoll, G. T. in *Handbook of Neural Activity Measurements* (eds Brette, R. & Destexhe, A.) 92–135 (Cambridge Univ. Press, 2012).
90. Fries, P. Neuronal gamma-band synchronization as a fundamental process in cortical computation. *Annu. Rev. Neurosci.* **32**, 209–224 (2009).
91. Markram, H. The blue brain project. *Nature Rev. Neurosci.* **7**, 153–160 (2006).
92. Lang, S., Dercksen, V. J., Sakmann, B. & Oberlaender, M. Simulation of signal flow in 3D reconstructions of an anatomically realistic neural network in rat vibrissal cortex. *Neural Netw.* **24**, 998–1011 (2011).
93. Gerstner, W. & Kistler, W. M. *Spiking Neuron Models: Single Neurons, Populations, Plasticity* (Cambridge Univ. Press, 2002).
94. Potjans, T. C. & Diesmann, M. The cell-type specific cortical microcircuit: relating structure and activity in a full-scale spiking network model. *Cereb. Cortex* http://dx.doi.org/10.1093/cercor/bhs358 (2012).
95. Phoka, E., Wildie, M., Schultz, S. R. & Barahona, M. Sensory experience modifies spontaneous state dynamics in a large-scale barrel cortical model. *J. Comput. Neurosci.* **33**, 323–339 (2012).
96. Bazhenov, M. *et al.* Model of transient oscillatory synchronization in the locust antennal lobe. *Neuron* **30**, 553–567 (2001).
97. Ursino, M. & La Cara, G. E. Travelling waves and EEG patterns during epileptic seizure: analysis with an integrate-and-fire neural network. *J. Theor. Biol.* **242**, 171–187 (2006).
98. Buehlmann, A. & Deco, G. The neuronal basis of attention: rate versus synchronization modulation. *J. Neurosci.* **28**, 7679–7686 (2008).
99. Beim Graben, P. & Rodrigues, S. A biophysical observation model for field potentials of networks of leaky integrate-and-fire neurons. *Front. Comput. Neurosci.* **6**, 100 (2012).
100. Hämäläinen, M., Hari, R., Ilmoniemi, R., Knuutila, J. & Lounasmaa, O. Magnetoencephalography theory, instrumentation, and applications to noninvasive studies of the working human brain. *Rev. Mod. Phys.* **65**, 413–497 (1993).
101. Freeman, W. J. Use of spatial deconvolution ot compensate for distortion of EEG by volume conduction. *IEEE Trans. Biomed. Eng.* **27**, 421–429 (1980).
102. Bonjean, M. *et al.* Interactions between core and matrix thalamocortical projections in human sleep spindle synchronization. *J. Neurosci.* **32**, 5250–5263 (2012).
103. Ulbert, I., Halgren, E., Heit, G. & Karmos, G. Multiple microelectrode-recording system for human intracortical applications. *J. Neurosci. Methods* **106**, 69–79 (2001).
104. Cash, S. S. *et al.* The human K-complex represents an isolated cortical down-state. *Science* **324**, 1084–1087 (2009).
105. Rappelsberger, P., Pockberger, H. & Petsche, H. Current source density analysis: methods and application to simultaneously recorded field potentials of the rabbit's visual cortex. *Pflugers Arch.* **389**, 159–170 (1981).
106. Swadlow, H. A., Gusev, A. G. & Bezdudnaya, T. Activation of a cortical column by a thalamocortical impulse. *J. Neurosci.* **22**, 7766–7773 (2002).
The introduction of spike-triggered LFP analysis to probe the LFP and CSD signatures of synaptic projections from individual neurons — in this case, the signatures in sensory neocortex following action potentials in a single thalamocortical neuron.
107. Jin, J., Wang, Y., Swadlow, H. A. & Alonso, J. M. Population receptive fields of ON and OFF thalamic inputs to an orientation column in visual cortex. *Nature Neurosci.* **14**, 232–238 (2011).
108. Leski, S. *et al.* Inverse current-source density method in 3D: reconstruction fidelity, boundary effects, and influence of distant sources. *Neuroinformatics* **5**, 207–222 (2007).
109. Potworowski, J., Jakuczun, W., Leski, S. & Wojcik, D. Kernel current source density method. *Neural Comput.* **24**, 541–575 (2012).
110. Lakatos, P. *et al.* An oscillatory hierarchy controlling neuronal excitability and stimulus processing in the auditory cortex. *J. Neurophysiol.* **94**, 1904–1911 (2005).
111. Lakatos, P., Karmos, G., Mehta, A. D., Ulbert, I. & Schroeder, C. E. Entrainment of neuronal oscillations as a mechanism of attentional selection. *Science* **320**, 110–113 (2008).
112. Mitra, P. & Bokil, H. *Observed Brain Dynamics* (Oxford Univ. Press, 2008).
113. Steriade, M. & Hobson, J. Neuronal activity during the sleep-waking cycle. *Prog. Neurobiol.* **6**, 155–376 (1976).
114. Basar, E. *EEG-Brain Dynamics: Relation Between EEG and Brain Evoked Potentials* (Elsevier/North-Holland Biomedical Press, 1980).
115. Gawne, T. J. & Richmond, B. J. How independent are the messages carried by adjacent inferior temporal cortical neurons? *J. Neurosci.* **13**, 2758–2771 (1993).
116. Pola, G., Thiele, A., Hoffmann, K. P. & Panzeri, S. An exact method to quantify the information transmitted by different mechanisms of correlational coding. *Network* **14**, 35–60 (2003).
117. Schneidman, E., Bialek, W. & Berry, M. J. Synergy, redundancy, and independence in population codes. *J. Neurosci.* **23**, 11539–11553 (2003).
118. Shannon, C. E. A mathematical theory of communication. *Bell Syst. Tech. J.* **27**, 623–656 (1948).
119. Quian Quiroga, R. & Panzeri, S. Extracting information from neuronal populations: information theory and decoding approaches. *Nature Rev. Neurosci.* **10**, 173–185 (2009).
120. Bartos, M., Vida, I. & Jonas, P. Synaptic mechanisms of synchronized gamma oscillations in inhibitory interneuron networks. *Nature Rev. Neurosci.* **8**, 45–56 (2007).
121. Magri, C., Mazzoni, A., Logothetis, N. K. & Panzeri, S. Optimal band separation of extracellular field potentials. *J. Neurosci. Methods* **210**, 66–78 (2012).
122. Gieselmann, M. A. & Thiele, A. Comparison of spatial integration and surround suppression characteristics in spiking activity and the local field potential in macaque V1. *Eur. J. Neurosci.* **28**, 447–459 (2008).
Using LFPs recorded from the primary visual cortex during the presentation of visual stimuli of variable size, the authors show that the neural generators of bands of the extracellular signal that are highly correlated in most conditions (such as gamma oscillations and spiking activity) can be dissociated by careful stimulus manipulations.
123. Mallat, S. G. & Zhang, Z. Matching pursuits with time-frequency dictionaries. *IEEE Trans. Signal Process.* **41**, 3397–3415 (1993).
124. Ray, S., Crone, N. E., Niebur, E., Franaszczuk, P. J. & Hsiao, S. S. Neural correlates of high-gamma oscillations (60–200 Hz) in macaque local field potentials and their potential implications in electrocorticography. *J. Neurosci.* **28**, 11526–11536 (2008).
125. Lee, D. D. & Seung, H. S. Learning the parts of objects by non-negative matrix factorization. *Nature* **401**, 788–791 (1999).
126. Logothetis, N. K. *et al.* Hippocampal–cortical interaction during periods of subcortical silence. *Nature* **491**, 547–553 (2012).
By combining functional imaging with recordings and analysis of LFPs, this study demonstrates that sharp-wave ripple complexes, but not other LFP events, are associated with widespread up- and downregulation of cortical and subcortical activity, respectively.
127. Tye, K. M. & Deisseroth, K. Optogenetic investigation of neural circuits underlying brain disease in animal models. *Nature Rev. Neurosci.* **13**, 251–266 (2012).
128. Beltramo, R. *et al.* Layer-specific excitatory circuits differentially control recurrent network dynamics in the neocortex. *Nature Neurosci.* **16**, 227–234 (2013).
A study in which optogenetic techniques are used to establish a causal demonstration that excitatory circuits located in distinct cortical layers exert differential control on spontaneous low-frequency LFPs.
129. Anastassiou, C. A., Perin, R., Markram, H. & Koch, C. Ephaptic coupling of cortical neurons. *Nature Neurosci.* **14**, 217–223 (2011).
130. Thut, G., Schyns, P. G. & Gross, J. Entrainment of perceptually relevant brain oscillations by non-invasive rhythmic stimulation of the human brain. *Front. Psychol.* **2**, 170 (2011).
131. Denker, M. *et al.* The local field potential reflects surplus spike synchrony. *Cereb. Cortex* **21**, 2681–2695 (2011).
132. Makarov, V. A., Makarova, J. & Herreras, O. Disentanglement of local field potential sources by independent component analysis. *J. Comput. Neurosci.* **29**, 445–457 (2010).
133. Leski, S., Kublik, E., Swiejkowski, D. A., Wrobel, A. & Wojcik, D. K. Extracting functional components of neural dynamics with independent component analysis and inverse current source density. *J. Comput. Neurosci.* **29**, 459–473 (2010).
134. Friston, K. J. *et al.* Classical and Bayesian inference in neuroimaging: applications. *Neuroimage* **16**, 484–512 (2002).
135. Friston, K., Mattout, J., Trujillo-Barreto, N., Ashburner, J. & Penny, W. Variational free energy and the Laplace approximation. *Neuroimage* **34**, 220–234 (2007).
136. Moran, R. J. *et al.* Bayesian estimation of synaptic physiology from the spectral responses of neural masses. *Neuroimage* **42**, 272–284 (2008).
This study establishes the technology of inversion (or data fitting) of models of neural masses to infer synaptic physiology from measures of LFP spectra.
137. Deco, G., Jirsa, V. K., Robinson, P. A., Breakspear, M. & Friston, K. The dynamic brain: from spiking neurons to neural masses and cortical fields. *PLoS Comput. Biol.* **4**, e1000092 (2008).
138. Moran, R. J. *et al.* Dynamic causal models of steady-state responses. *Neuroimage* **44**, 796–811 (2009).
139. Brunel, N. & Wang, X. J. What determines the frequency of fast network oscillations with irregular neural discharges? I. Synaptic dynamics and excitation–inhibition balance. *J. Neurophysiol.* **90**, 415–430 (2003).
140. Wang, X. J. Neurophysiological and computational principles of cortical rhythms in cognition. *Physiol. Rev.* **90**, 1195–1268 (2010).
141. Ostojic, S. & Brunel, N. From spiking neuron models to linear-nonlinear models. *PLoS Comput. Biol.* **7**, e1001056 (2011).
142. Nordlie, E., Tetzlaff, T. & Einevoll, G. T. Rate dynamics of leaky integrate-and-fire neurons with strong synapses. *Front. Comput. Neurosci.* **4**, 149 (2010).
143. Tetzlaff, T., Helias, M., Einevoll, G. T. & Diesmann, M. Decorrelation of neural-network activity by inhibitory feedback. *PLoS Comput. Biol.* **8**, e1002596 (2012).
144. Ledoux, E. & Brunel, N. Dynamics of networks of excitatory and inhibitory neurons in response to time-dependent inputs. *Front. Comput. Neurosci.* **5**, 25 (2011).
145. Barbieri, F., Mazzoni, A., Logothetis, N. K., Panzeri, S. & Brunel, N. The dynamics of local field potential in monkey primary visual cortex under naturalistic stimulation is well captured by a model network of excitatory and inhibitory integrate-and-fire neurons. *Soc. Neurosci. Abstr.* 483.402 (2011).
146. Friston, K. J. *et al.* DCM for complex-valued data: cross-spectra, coherence and phase-delays. *Neuroimage* **59**, 439–455 (2012).
147. Blomquist, P. *et al.* Estimation of thalamocortical and intracortical network models from joint thalamic single-electrode and cortical laminar-electrode recordings in the rat barrel system. *PLoS Comput. Biol.* **5**, e1000328 (2009).
148. Lisman, J. The theta/gamma discrete phase code occuring during the hippocampal phase precession may be a more general brain coding scheme. *Hippocampus* **15**, 913–922 (2005).
149. Canolty, R. T. *et al.* High gamma power is phase-locked to theta oscillations in human neocortex. *Science* **313**, 1626–1628 (2006).
150. Fevotte, C., Bertin, N. & Durrieu, J. L. Nonnegative matrix factorization with the Itakura-Saito divergence: with application to music analysis. *Neural Comput.* **21**, 793–830 (2009).
151. Liutkus, A., Badeau, R. & Richard, G. Gaussian processes for underdetermined source separation. *IEEE Trans Signal Process.* **59**, 3155–3167 (2011).
152. Traub, R. D. *et al.* Single-column thalamocortical network model exhibiting gamma oscillations, sleep spindles, and epileptogenic bursts. *J. Neurophysiol.* **93**, 2194–2232 (2005).

153. Einevoll, G. T., Franke, F., Hagen, E., Pouzat, C. & Harris, K. D. Towards reliable spike-train recordings from thousands of neurons with multielectrodes. *Curr. Opin. Neurobiol.* **22**, 11–17 (2012).
154. Devor, A., Boas, D. A., Einevoll, G. T., Buxton, R. B. & Dale, A. M. in *Neural Metabolism* In Vivo (eds Choi, I.-Y. & Gruetter, R.) 433–500 (Springer, 2012).
155. Pearl, J. *Causality: Models, Reasoning, and Inference* (Cambridge Univ. Press, 2000).
156. Lizier, J. T. & Prokopenko, M. Differentiating information transfer and causal effect. *Eur. Phys. J. B* **73**, 605–615 (2010).
157. Goto, T. *et al.* An evaluation of the conductivity profile in the somatosensory barrel cortex of Wistar rats. *J. Neurophysiol.* **104**, 3388–3412 (2010).
158. He, B. & Lian, J. *Electrophysiological Neuroimaging in Neural Engineering* (Kluwer/Plenum, 2004).
159. Gratiy, S. L., Pettersen, K. H., Einevoll, G. T. & Dale, A. M. Pitfalls in the interpretation of multielectrode data: on the infeasibility of the neuronal current-source monopoles. *J. Neurophysiol.* **109**, 1681–1682 (2013).
160. Riera, J. & Cabo, A. Reply to Gratiy *et al.* *J. Neurophysiol.* **109**, 1684–1685 (2013).
161. Bedard, C. & Destexhe, A. Reply to Gratiy *et al.* *J. Neurophysiol.* **109**, 1683 (2013).
162. Rank, J. B. Specific impedance of rabbit cerebral cortex. *Exp. Neurol.* **7**, 144–152 (1963).
163. Nauhaus, I., Busse, L., Ringach, D. L. & Carandini, M. Robustness of traveling waves in ongoing activity of visual cortex. *J. Neurosci.* **32**, 3088–3094 (2012).
164. Ray, S. & Maunsell, J. H. Network rhythms influence the relationship between spike-triggered local field potential and functional connectivity. *J. Neurosci.* **31**, 12674–12682 (2011).
165. Granger, C. Investigating causal relations by econometric models and cross-spectral methods. *Econometrica* **37**, 424–438 (1969).
166. Schreiber, T. Measuring information transfer. *Phys. Rev. Lett.* **85**, 461–464 (2000).
167. Besserve, M., Scholkopf, B., Logothetis, N. K. & Panzeri, S. Causal relationships between frequency bands of extracellular signals in visual cortex revealed by an information theoretic analysis. *J. Comput. Neurosci.* **29**, 547–566 (2010).
168. Bosman, C. A. *et al.* Attentional stimulus selection through selective synchronization between monkey visual areas. *Neuron* **75**, 875–888 (2012).
A study reporting that inter-areal feedforward causal influences from cortical area V1 to cortical area V4 are frequency-dependent and are strongest in the gamma band.
169. Roelfsema, P. R. *et al.* Alpha and gamma oscillations as markers of feedforward and feedback processing in areas V1 and V4 of monkey visual cortex. *Soc. Neurosci. Abstr.* 623.03 (2012).
170. Zanos, T. P., Mineault, P. J. & Pack, C. C. Removal of spurious correlations between spikes and local field potentials. *J. Neurophysiol.* **105**, 474–486 (2011).
171. Rasch, M., Logothetis, N. K. & Kreiman, G. From neurons to circuits: linear estimation of local field potentials. *J. Neurosci.* **29**, 13785–13796 (2009).
172. Harris, K. D. & Thiele, A. Cortical state and attention. *Nature Rev. Neurosci.* **12**, 509–523 (2011).
173. Mainen, Z. F. & Sejnowski, T. J. Influence of dendritic structure on firing pattern in model neocortical neurons. *Nature* **382**, 363–366 (1996).

Acknowledgements
We thank H. Lindén, K. H. Pettersen, C. Magri, F. Szymanski and J. Schnupp for help with the figures, and J. Assad, M. Diamond, N. Brunel, A. Mazzoni and A. Marreiros for precious comments on the manuscript. This work was supported by the Research Council of Norway (eVita, NOTUR, NevroNor and ISP-Fysikk), the Max Planck Society in Germany, the Compagnia di San Paolo in Italy, the SI-CODE (FET-Open, FP7-284533) and BrainScaleS (FP7-269921) projects within the Seventh Framework for Research, and the People Programme (Marie Curie Actions) ABC (FP7-290011) project of the European Union's Seventh Framework Programme FP7 2007-2013 under grant agreement PITN-GA-2011-290011. In addition, this work was part of the research programme of the Bernstein Center for Computational Neuroscience, Tübingen, funded by the German Federal Ministry of Education and Research (BMBF; FKZ: 01GQ1002).

Competing interests statement
The authors declare no competing financial interests.

FURTHER INFORMATION

INCF Software Center: http://software.incf.org/
NeuroMorph.org: http://neuromorpho.org/neuroMorpho/index.jsp
Spike Sorting Evaluation Project: http://spike.g-node.org/
The Human Brain Project: https://www.humanbrainproject.eu/

SUPPLEMENTARY INFORMATION

See online article: S1 (box) | S2 (box)

ALL LINKS ARE ACTIVE IN THE ONLINE PDF